Paleomagnetic study from the Gyeongsang Basin, southeastern part of the Korean Peninsula: Origin of the magnetization of red beds and tectonic implication

Masato Tamai

A doctoral dissertation

submitted to Kyoto University

December, 1997

Abstract

A paleomagnetic study with a rock magnetic study was performed on the Cretaceous sedimentary rocks in the Gyeongsang Basin, southeastern part of the Korean Peninsula. Red beds of 40 sites and non-red sedimentary rocks from of 8 sites were analyzed.

Thermal demagnetization for the red beds revealed two magnetic components, either carried by hematite. The component A is obtained at lower unblocking temperature below ~640°C, and the component B resides in much higher unblocking temperature range up to 680°C. These two component are likely chemical remanent magnetization (CRM) and (post-)detrital remanent magnetization (DRM) origin of hematite. Rock magnetic investigation elucidated rock magnetic property of each component and its implication with the paleomagnetic directions. Thermal and alternating field demagnetization revealed that CRM had lower unblocking temperature but higher coercivity than that of DRM. Magnetic anisotropy suggests that DRM is probably controlled by sedimentary fabric resulting in inclination shallowing.

The component A is suggested to be acquired after the tilting during the Cretaceous Normal Superchron (middle to late Cretaceous). It is possible to regard the direction of the component A representing paleomagnetic direction from the Gyeongsang Basin at the late Cretaceous. Mean direction of the component A is $D=11.8°$, $I=56.9°$ and $\alpha_{95}=5.3°$, corresponding to a paleopole at 80.2°N, 201.5°E and $A_{95}=6.4°$. Much concentrated direction provides the reliable paleopole, which is consistent with those from the main part of the eastern Asia (the North China Block and the Yangtze Block). This indicates that the Korean Peninsula was associated with the main part of the eastern Asia since the late Cretaceous time, and had tectonically behaved as a stable continent even when the Japan Arc was torn off from the Korean Peninsula.

The component B is DRM origin acquired at the early Cretaceous time, but this is biased both by the contamination of the component A and by the inclination shallowing. We cannot suggest the early Cretaceous paleomagnetic direction on the basis of the component B, although this was determined after precise thermal demagnetization.

Contents

Introduction

Paleomagnetic study of the eastern Asia has been extensively investigated since the last twenty years. These data were compiled by Enkin et al. [1992]. The purpose of the studies are mainly to establish the reliable paleomagnetic poles for each age stage and to solve the tectonic history of the eastern Asia. Paleomagnetic study of the Korean Peninsula has been also approached to contribute the tectonic history of Asia. All pre-Cretaceous paleomagnetic studies has been reported that the rocks of the Okcheon Folded Belt in the Korean Peninsula suffered strong remagnetization, probably after the Cretaceous [Otofuji et al., 1986; Shibuya et al., 1988; Kim and Van der Voo, 1990; Doh and Piper, 1994]. The timing of remagnetization has been controversial, however, In some of those studies, the primary magnetization are believed to be revealed successfully, because the obtained paleomagnetic directions deviate largely from the directions of remagnetization and/or of geocentric axial dipole field. However, Lee et al. [1996] claimed that the paleomagnetic directions must be obtained with a careful rock magnetic analysis.

Cretaceous paleomagnetic studies in the southern part of the Korean Peninsula have been done for these several decades. Pioneering study was performed on igneous rocks: Kienzle and Scharon [1966] reported the results from andesites, dacites and rhyolites. Ito and Tokieda [1980] reported the results of granites. Their paleomagnetic directions, however, were reported only based on the directions without or after insufficient alternating field (AF) demagnetization (40 mT or 10mT). Further no field test was applied.

1

Otofuji et al. [1983] and Otofuji et al. [1986] studied the Cretaceous sedimentary rocks of the Gyeongsang Basin. They considered the directions after AF demagnetization of 30 mT or 10 mT as reliable primary magnetizations, after stepwise AF and thermal demagnetizations of pilot samples. Detailed study of the identical strata was carried out by Lee et al. [1987]. They found that the Cretaceous rocks were also remagnetized like the pre-Cretaceous rocks. They obtained characteristic component with careful thermal demagnetization, while they did not consider the variation of magnetic minerals carrying natural remanent magnetization (NRM). Their characteristic component was determined at different unblocking temperature ranges disregarding remanence carriers. Although the overprinted magnetization survived for thermal demagnetization up to 650°C at some sites of red beds, they determined characteristic component below 650°C for the rest of sites of red beds. Although their results passed a fold test and a reversal test [Butler, 1992], their results were not supported by any rock magnetic experiments. The age of the fold event was not given, and remagnetization might have occurred over normal and reversed chrons. Otherwise the directional data are highly possible to be suffered from the wide spread remagnetization in eastern Asia [Moreau et al., 1987]. It is necessary to re-examine the previous results from the view point of NRM acquisition in red beds with detailed rock magnetic experiments.

Red beds are one of the most useful targets for paleomagnetism because of their stable NRM carried by hematite. They have been extensively studied for various purposes, such as magnetostratigraphy and tectonics by many paleomagnetists. However the NRM in red beds is sometimes problematic upon the mechanism and timing of magnetic

2

acquisition [Butler, 1992]. Origin of the magnetization carried by hematite in red beds are generally interpreted as (post-)detrital remanent magnetization (DRM) [e.g. Elston and Purucker, 1979; Steiner, 1983] or chemical remanent magnetization (CRM) [e.g. Turner, 1979; Channell et al., 1982; Hodych et al., 1985]. The former is carried by larger detrital grains (specularite), and the latter is by smaller authigenic grains (pigment) [Tauxe et al., 1980]. In many cases, either grains coexist in red bed, although the rock color, after which red beds are called, is attributed to the pigmentary hematite. To solve the problems of NRM acquisition of red beds, rock magnetic experiments and/or microscopic observation have been conducted for hematite [e.g. Collinson, 1974; Dekkers and Linssen, 1989; Hejda et al., 1992]. Dunlop [1970] pointed out that the magnetic properties of hematite are strongly concerned not only with grain size but also with defect moments and magnetocrystalline anisotropy. These various factors of hematite make paleomagnetism of red beds complicated.

The separation of DRM and CRM in red beds has been tried by several authors. It was shown that the magnetization of smaller pigmentary hematite had higher coercivity and lower unblocking temperature than those of larger specularite [Brooks and O'Reilly, 1970; Tauxe et al., 1980; Channell et al., 1982; Jackson and Van der Voo, 1986]. Lee et al. [1996] conducted detailed thermal demagnetization, whose interval were 3°C to 5°C above 670°C, based on the minor difference of unblocking temperature. Roy and Park [1972] referred that a part of CRM was not cleaned by thermal demagnetization, and they employed a chemical demagnetization by which smaller grains were leached by acid.

Hematite is also known as strongly anisotropic mineral. The crystalline anisotropy is so high for its basal plane that its shape anisotropy can be ignored [Tarling and Hrouda, 1993]. Tauxe and Kent [1984] observed that the inclination shallowing occurred for DRM carried by hematite. The coupling of the anisotropy of magnetic susceptibility (AMS) with DRM direction were observed both for synthetic sediments containing hematite and for natural red beds [Løvlie and Torsvik, 1984; Garcés et al., 1996]. This is evidenced by inclination shallowing due to the compaction of sediments after deposition. Bazhenov et al. [1995], on the other hand, suggested that compaction effect also would operate on the CRM direction to reduce inclination. They observed that the older CRM of hematite showed shallower inclination. This phenomenon could be interpreted as diagenetic compaction of non-magnetic minerals which was coated by authigenic hematite [Sun and Kodama, 1992].

As described above, the rock magnetic property cannot be ignored for the study of paleomagnetic direction of red beds. In this study, the primary purpose is to obtain a reliable Cretaceous paleomagnetic direction from the Gyeongsang Basin of the Korean Peninsula. And the rock magnetic study of red beds is also performed to help interpretation of obtained directional data.

Geological setting and sampling

The Korean Peninsula is situated on the eastern flank of the Asian continent (Fig. 1a). It basically consists of continental crust of the Precambrian basement, continued by that of main part of Asia to the north and the west [Lee (ed.), 1987]. To the east, the peninsula faces the Japan Sea which was opened rapidly as the back arc basin in the middle Miocene [e.g. Otofuji, 1996].

The geology of the Korean Peninsula was compiled by Lee (ed.) [1987]. Main geologic history of the southern part of the Korean Peninsula since the Late Mesozoic was summarized as follows: In the late Jurassic, the Daebo Orogeny was occurred widely in the peninsula. The Jurassic granites intruded at this time. After fading this event, large trough was formed in the southeastern part of the peninsula in front of the Ryeongnam Massif, and sedimentation had started in this trough at the early Cretaceous. This trough generated along the Ryeongnam Massif and enhanced easterly correlated with the tectonic extension at that time. In the middle to late Cretaceous, volcanic activity occurred and granite intrusion followed the volcanism. They are called the Yucheon Volcanism and the Bulguksa Disturbance, respectively. These events continued to the Paleogene. At the end of the Cretaceous period, the Korean Peninsula had been uplifted as a land except for the eastern coastal region. The Cretaceous basins were extinguished by this time and few Tertiary sediments were distributed except for the eastern coastal region. In Cenozoic, large strike-slip faults with NNE-SSW trend have been active up to the present day in the southeastern part.

5

The Gyeongsang Basin, widely occupied southeastern part of the Korean Peninsula (Fig. 1b), was formed during the Cretaceous period as mentioned above. The basin was formed as trough where non-marine sediments, volcanoclastic and volcanic rocks were deposited at the fluvio-lacustrine condition. The Cretaceous strata in the basin overlie the Precambrian gneisses or the Jurassic granites unconformably, partly with the Jurassic sediments, and have the thickness of more than 10 km. Now these strata are dipping gently east to southeast. The sequences formed in that time in South Korea are called the Gyeongsang Supergroup. These system is typically divided into three groups and each group comprises several formations (Fig. 2). The Shindong Group, the lowest part of the basin, was composed of the Nagtong, Hasandong and Jinju Formations in ascending order. These strata comprise continental sediments such as sandstone, shale, conglomerate and marl. Some banded red beds, which are nearly drab colored, intervene in the Hasandong Formation. The Jinju Formation does not contain any red sediment but mainly gray sandstones or black shale. The Hayang Group overlies the Shindong Group. It is also composed of continental sediments. The difference from the Shindong Group is that the sediments are of volcanic origin and that the purplish colored red beds are predominant. This group is divided into the Chilgok, Shilla, Haman and Jindong Formations in ascending order. The Hayang Group is generally unconformably overlain by the Yucheon Group. The Hayang Group is characterized by the dominance of volcanic rocks.

The ages of sequences are directly determined by fossils and indirectly by the stratigraphic correlation with the igneous rocks whose age were determined radiometrically [Lee (ed.), 1987]. Based on the

6

biostratigraphy with the assistance of the geologic time scale by Harland et al. [1990], the basal unit of the Gyeongsang Supergroup is Valanginian (138-131 Ma) or Hauteruvian (131-125 Ma) and that the uppermost part of the Hayang Group is Aptian (119-113 Ma) to early Albian (113-97.5 Ma). These age are well consistent with the radiometric (K-Ar and/or Rb-Sr) ages. The Daebo Granite which predated the sedimentation of the Gyeongsang Supergroup is 170 to 138 Ma in Ryeongnam Massif. The Yucheon Group underlain by the Hayang Group is around 85 to 60 Ma, and the Bulguksa Granite which intruded the Yucheon Group is around 115 to 68 Ma in the Gyeongsang Basin.

Sampling was carried out around Jinju (35.2°N, 128.0°E) and Goreong (35.7°N, 128.3°E) in the Gyeongsang Basin (Fig. 1b). Cretaceous sedimentary rocks were collected for paleomagnetic study. Total 51 sites of the Hasandong, Jinju, Chilgok and Shilla Formations were analyzed in this study (Table 1, Fig. 3). These were formed in the early Cretaceous, corresponding to the age before the Cretaceous Normal Superchron (Fig. 2). Samples were mainly red sediments, except for three sites of the Hasandong Formation and all of the Jinju Formation.

About five block samples, oriented with a magnetic compass, were collected in a site within a few meters height and several meters wide to stratigraphic horizon. The bedding attitude was measured with a magnetic compass at each site. Those strata dip gently (<20° at Jinju area and <30° at Goreong area) to east to southeast (Table 1). All field-measured orientations were corrected by using the local geomagnetic declination (353°) based on International Geomagnetic Reference Field of 1994 [IAGA Division V, 1995].

7

Laboratory procedures and analytical methods

One or more oriented core specimens, 23 mm in diameter and about 22 mm in height, were prepared from each hand sample. These specimens were used for measurements of NRM, AMS, and anisotropy of isothermal remanent magnetization (IRM). Some of the samples were crushed into small pieces (~5 mm) with a mortar and pestle made of tungsten-carbide. These fragments were used for rock magnetic measurements.

NRM was measured with a cryogenic magnetometer (ScT C-112). All samples were treated by stepwise thermal demagnetization to reveal remanence components of which NRM consisted. Samples were heated more than 30 minutes at the set temperature and cooled down to the room temperature in the furnace shielded from the ambient magnetic field, in which the residual field is lower than 20 nT.

Low-field susceptibility was measured after each step of thermal demagnetization on a magnetic susceptibility meter of Bartington M.S.2. in order to monitor the alteration of magnetic minerals during thermal demagnetization. Thermomagnetic analysis was performed with a semi-horizontal automatic thermomagnetic balance. Induced magnetization in the magnetic field of 0.85 T was monitored during heating up to the 700°C and cooling to the room temperature in air or in Argon gas.

Some specimens were treated by stepwise AF demagnetization using 2G600 Automatic Sample Degaussing System with a 3-axis sample tumbler. Although AF demagnetization was ineffective to reveal the

remanence, it is helpful to examine the rock magnetic properties of samples.

Acquisition of IRM was performed on a pulse magnetizer (MMPM-9). Small fragment was progressively applied the field up to 9 T and then was applied backfield. Its remanence at each field step was measured with the cryogenic magnetometer. Core specimen was also treated with similar procedure in order to check the anisotropy of IRM. These IRMs were acquired to the 2.8 T and measured with a spinner magnetometer (Natsuhara Giken Aspin). Degree of anisotropy of IRM was evaluated by the IRM acquisition curves to the three orthogonal axes of sample. Two axes are in bedding plain and the rest is perpendicular to the bedding plain. Magnetic field of 2.8 T was first applied to a sample in one direction and back field was applied stepwisely. The resultant IRM was measured at each step of back-field application. After this, same process was repeated to other two directions, individually. As the first-ordered approximation of anisotropy, the ratio of vertical IRM (IRMv) to horizontal IRM (IRMh) is calculated for each samples. IRMv was plotted against IRMh for same applied field, and IRMv/IRMh was estimated using the slope of a least-squares-fit line for each of these plot [Hodych and Buchan, 1994].

Low-temperature magnetic property below room temperatures to 10 K or 5 K was measured with a Quantum Design's Magnetic Property Measurements System (MPMS-2) at the Low-Temperature Laboratory of Kyoto University. Two mode of experiments were performed. First is warming mode: The sample which acquired IRM for applied field of 1 T at 10 K (or 5K) were demagnetized thermally to the room temperature (300 K). Second is cooling-warming mode: The sample which acquired

IRM for applied field of 1 T (or 9.25 T with a pulse magnetizer) at room temperature was cooled down to 10 K and then warmed to the room temperature in the field free space. During these procedures, the remanence intensity was monitored in order to observe each intrinsic phase transition for some magnetic minerals.

AMS was measured with a Kappabridge KLY-3S susceptibility bridge at Faculty of Integrated Human Sciences, Kyoto University. The data were analyzed following the method of Tarling and Hrouda [1993]. Principal susceptibilities of $K_1 \geq K_2 \geq K_3$ were determined, and degree (Pj) and shape parameter (T) of AMS were given by

$$Pj = \exp\sqrt{2\left[(\eta_1 - \eta_m)^2 + (\eta_2 - \eta_m)^2 + (\eta_3 - \eta_m)^2\right]}$$

and

$$T = (2\eta_2 - \eta_1 - \eta_3)/(\eta_1 - \eta_3),$$

where

$$\eta_1 = \ln K_1; \eta_2 = \ln K_2; \eta_3 = \ln K_3; \eta_m = \sqrt[3]{\eta_1 \cdot \eta_2 \cdot \eta_3}.$$

For paleomagnetic analysis, orthogonal vector diagram was used to assess the behavior of individual specimens for demagnetization [Zijderveld, 1967]. Kirschvinc's principal component analysis [Kirschvinc, 1980] was used to determine the direction of remanence component. Mean direction was analyzed based on Fisher statistics [Fisher, 1953].

Rock magnetic properties of red beds

Hasandong Formation

NRM behavior for thermal demagnetization

NRM are enough strong ($>3 \times 10^{-8}$ Am^2, Fig. 4) to measure with a cryogenic magnetometer. All samples were subjected to the stepwise thermal demagnetization.

Remanence of the samples from Jinju area showed stable behavior for thermal demagnetization up to the 680°C. The maximum unblocking temperature was around 675°C. This is identical to the Curie temperature of hematite. During the stepwise thermal demagnetization, intensity did not decrease largely up to ~350°C, and gradually decreased by ~650°C. Finally intensity sharply decayed at ~675°C (Fig. 5). Little NRM was carried by magnetite, because the intensity decreased gradually through the Curie temperature of magnetite (~580°C). The magnetic carrier of NRM is mainly hematite with wide unblocking temperature ranges.

The samples from Goreong area showed that the NRM behavior below 640°C for thermal demagnetization are almost same as the samples from Jinju area (Fig. 6). The magnetization above 640°C, however, often showed the erratic behavior (Fig. 6c and 6d).

One or two linear segments on orthogonal vector diagram were visibly revealed with a stepwise thermal demagnetization after cleaning of small viscous remanence. Two segments are distinguishable at the temperature of 620~660°C (Fig. 5d, 5e and 5f). It is defined by the difference of unblocking temperature that component A is carried by

11

low-unblocking temperature (~640°C) hematite with little magnetite and that component B is carried by high-unblocking temperature hematite whose unblocking temperature is identical with its Curie temperature (675°C). The characters of the directions of each component are mentioned later.

Magnetic stability for thermal treatments

Low-field susceptibility was measured at room temperature after each steps of thermal demagnetization (Fig. 7 and 8). They are stable or a little decrease up to 450°C. Above 500°C, susceptibility of some samples increased suddenly. Increasing degrees are different within site. The increase of susceptibility is due to thermal alterations of samples [van Velzen and Zijderveld, 1992]. The higher the susceptibility became, the easier viscous remanent magnetization (VRM) was acquired in the laboratory. Actually on the remanence measurements it took several tens of minutes to reduce VRM component by keeping a sample in the zero-field space in magnetometer. The magnetic behavior for thermal demagnetization does not depend on the change of susceptibility value. Even in the case that the magnetic susceptibility increased largely, remanence did not always show erratic behavior. Such thermal alteration of red beds was reported so far [e.g. Lee et al., 1996] and was accounted for the production and/or growth of ferrimagnetic impurities, probably ultra-fine (superparamagnetic) magnetite and/or hematite grains on heating [Dekkers and Linssen, 1989; Dekkers, 1990; van Velzen and Zijderveld, 1992]. However, superparamagnetic minerals does not influence the measurements of remanence except for time consumption.

Results of the experiment using a thermomagnetic balance well explain the NRM behaviors for thermal demagnetization. The thermomagnetic curves indicate that the dominant magnetic mineral is hematite. Magnetite or maghemite is not significant. The samples from Jinju area showed the reversible curves after heating up to 700°C as shown in Fig. 9. The cooling curve is almost identical with the heating curve. On the other hand, the samples from Goreong area often suggested mineral alteration caused by the laboratory heating. The induced magnetization increased largely after the heating due to newly formed magnetic minerals (Fig. 10a). This thermal alteration made difficult to identify the component B for the samples from Goreong area. Newly formed magnetic minerals should disturb the component B of weak magnetization.

NRM behavior for AF demagnetization and subsequent thermal demagnetization

Stepwise AF demagnetization was applied to pilot sample. NRM was not cleaned completely up to 180 mT, but 10% to 55% of NRM was demagnetized. This indicates that NRM is carried by the magnetic minerals with various coercivity ranges and that these ranges are different from sample to sample.

The NRM intensity was gradually decreased with AF demagnetization. After the removal of very soft magnetization (below 40 mT), linear magnetic direction was recognized (Fig. 11a and 11b). The directions are intermediate between those of the components A and B determined with the thermal demagnetization (Fig. 11c and 11d). This

13

indicates that both the components A and B are cleaned simultaneously by AF demagnetization of 40 mT to 180 mT.

Following AF demagnetization to 180 mT, stepwise thermal demagnetization was applied to the samples which showed clear two magnetic components by thermal demagnetization. The remaining magnetization after AF demagnetization was almost destroyed at about 640°C and showed erratic behavior above this (Fig. 11a and 11b). The directions for thermal demagnetization (~640°C) after AF demagnetization are well consistent to those of the component A of thermal demagnetization only (Fig. 11c and 11d). This means that the component B is demagnetized almost completely by AF demagnetization. It can be concluded that the component A has variable coercivity whereas the component B is dominated by relatively lower coercivity fraction.

IRM acquisition and back-field demagnetization

Stepwise acquisition of IRM for applied field up to 9 T was performed on a pulse magnetizer at room temperature. The high field more than 3 T is necessary to saturate the magnetization (Fig. 12). The lower coercivity of remanence is probably due to the contamination of magnetite (Fig. 12d).

Low-temperature treatment of IRM

IRM behavior below room temperature was observed for some samples. Applied field was 1 T except for one measurement. Although 1 T was insufficient to saturate hematite, about 80% of saturation magnetization was acquired (Fig. 12).

The Morin transition of hematite, at 253 K for the pure (crystal) hematite, was not shown clearly for the experiments of both warming mode and cooling-warming mode (Fig. 13). This is a common feature for hematite in sediments, especially for fine-grained hematite. Dekkers and Linssen [1989] found that the authigenic hematite at low temperature origin lacked sharp Morin transition which was observed in the detrital hematite of high temperature origin. The lack of Morin transition was explained by the existence of defect moment [Dekkers and Linssen, 1989]. At cooling-warming mode, gradual decrease of the magnetization was observed in wide temperature range when cooled down to 10 K. About 15~25% of isothermal remanence were lost at 10 K. More than 30% of the lost magnetization was recovered by heating to room temperature (Fig. 13d, 13e and 13f). This recovery is due to the memory effect of remanence of hematite [Nagata et al., 1964].

The Verwey transition of magnetite at 120 K was sometimes observed either mode of experiments (Fig. 13b, 13e and 13f). This indicates the trace existence of magnetite or maghemite [Nagata et al., 1964; Özdemir et al., 1993; Torii et al., 1996]. The low-temperature transition of pyrrhotite (30~34 K) was not observed at all [Rochette et al., 1990; Torii et al., 1996].

Anisotropy of magnetic susceptibility

AMS can indicate sedimentary fabric very well. The degree of anisotropy (Pj) is not very high and varies from 1.01 to 1.11 and the shape of anisotropy ellipsoid is dominantly oblate $(T>0)$ as shown in Fig. 14. Their minimum axes are almost perpendicular to bedding plane (Fig.14).

15

Anisotropy of IRM

The anisotropy of IRM relative to the bedding plain was shown cleanly (Fig. 15). The IRMs along two horizontal axes parallel to bedding plane are almost identical, but IRM along vertical axis is significantly small. This indicates the oblate anisotropy relative to the bedding plane. IRMv/IRMh is calculated for each samples at three coercivity windows; ≤ 0.3 T for lower-coercivity hematite and/or magnetite, 0.3~1 T for lower-coercivity hematite and ≥ 1 T for higher-coercivity hematite. This is listed in Table 2 with comparable values of AMS. IRMv/IRMh is 0.68 to 0.92 for lower-coercivity hematite. This ratio is lower than that of the other coercivity windows and that of AMS. The lower-coercivity hematite contributes largely to the anisotropy of IRM. This suggests that the anisotropic hematite grains of lower coercivity prefer to arrange their basal plane parallel to the bedding plane.

Tauxe et al. [1990] and Hodych and Buchan [1994] pointed out that the first direction of applied field tended to acquire a stronger remanence and that IRM anisotropy was often enhanced by the experimental method. This was not remarkable for this results, because the IRMhs to the first and the second directions for bedding plane are almost same.

Chilgok and Shilla Formations

NRM behavior for thermal demagnetization

NRM intensity and low-field susceptibility were fairly large rather than the Hasandong Formation, and larger NRM intensity associated with larger susceptibility within these formations (Fig. 4).

All samples were treated for stepwise thermal demagnetization. The samples with lower susceptibility yielded the similar results to the Hasandong Formation. Many samples, with higher susceptibility, showed that the intensity decayed sharply around 560~580°C (Fig. 16). This temperature is almost identical with the Curie temperature of magnetite. The unblocking temperature of hematite was also observed above 580°C, especially around 675°C, while hematite is less contributed for NRM intensity than magnetite.

After cleaning of viscous remanent magnetization below 300°C, single linear segment (component A) was observed on orthogonal vector diagram from almost all the samples. This was dominantly carried by magnetite and partly by low-temperature unblocking hematite. Remanence direction often became erratic after heating above 640°C, mainly due to weak magnetization compared to NRM. Despite of these behaviors, the component B above 640°C was observed for some samples.

Magnetic stability for thermal treatments

Low-field susceptibility at room temperature after each steps of thermal demagnetization are shown in Fig. 17. Increasing after 500°C was probably same phenomena as the Hasandong Formation. Gradual decreasing up to 680°C was also often observed (Fig. 17b). This suggests that the magnetite was oxidized to hematite due to the laboratory heating [Velzen and Zijderveld, 1992].

17

Thermomagnetic curves reveal that the existence of maghemite and magnetite. The heating track significantly fell down dramatically at around 350°C and 580°C (Fig. 18b). During the cooling process, recovery around 580°C was only observed. The decrease of remanence due to the maghemite transition was not recognized on thermal demagnetization of NRM. Although hematite was identified by thermal demagnetization, the induced magnetization carried by hematite seems to be masked by the large magnetization of magnetite and maghemite. The contamination of magnetite and maghemite are probably caused by the volcanic materials. Good correlation between NRM intensity and low-field susceptibility probably indicates that they depend on the amount of magnetite (Fig. 4).

Rock magnetic properties of the non-red sedimentary rocks

Hasandong Formation

The samples are coarse sandstones. NRM intensity and low-field susceptibility was very weak (Fig. 4), and the remanence showed erratic behavior both for thermal and AF demagnetizations. As no reliable data was obtained, no further discussion will be made.

Jinju Formation

Samples of fine grained sandstones, mudstones and shales from the Jinju Formation were treated with stepwise thermal demagnetization for all samples and stepwise AF demagnetization for additional samples.

NRM intensity decay curves by the thermal demagnetization were variable from site to site (Fig. 19). Stable single component whose maximum unblocking temperature was around 580°C was obtained from almost all the samples, except for one site (site of JJ045 in Fig. 19d). The maximum unblocking temperature indicates that the main carrier of NRM is magnetite. This was also shown by the presence of low-temperature Verwey transition (Fig. 20a).

Only one sample (JJ0393) showed reliable component of reversed polarity for both thermal and AF demagnetizations (Fig. 19e and 19f). Normal polarity component was obtained below 200°C and above 350°C

of thermal demagnetization. The polarity was reversed between $200°C$ to $350°C$. Normal polarity component was also obtained below 100 mT of AF demagnetization. Reversed polarity component remains after cleaning of the normal polarity component and was not demagnetized completely by 180 mT. These characters explain that the magnetization with reversed polarity is carried by the mineral(s) of higher coercivity and of middle unblocking temperature. Such magnetic minerals are possibly maghemite or hematite of low unblocking temperature. Thermomagnetic analysis showed mineral change to magnetite during heating above $450°C$ in air and after heating to $700°C$ in Argon gas (Fig. 20b and 20c). This is one of the evidence for existence of maghemite. Many samples showed that NRM intensity would not decay but increased a little during thermal demagnetization ($250°C$ to $350°C$) (Fig. 19b). This may suggest the existence of anti-parallel remanent component of very small intensity as shown in the case of JJ0393.

Paleomagnetic directions

Red beds

One or two linear remanent components were observed from each sample of red beds. The component A is common among all samples. This is carried by magnetite and/or low-temperature unblocking hematite. The component B is of high-temperature unblocking hematite, while some samples seems to be lacking for the component B.

The different direction between the components A and B is clearly visible on the orthogonal vector diagram for most of the samples of the Hasandong Formation in Jinju area (Fig. 5d, 5e and 5f). But even in the samples of this formation, the component B is occasionally difficult to identify with the Kirschvinc's principal component analysis [Kirschvinc, 1980] due to weak intensity of the component B relative to the component A and/or due to small angular difference between the components A and B. In order to obtain the components A and B successfully, the principal component analysis was applied to the thermal demagnetization results, divided by the temperature ranges below and above 640°C (partly 650°C due to skipping the demagnetization level of 640°C). The criteria for reliable component were determined that the maximum angular deviation of each component did not exceed 5.0° and 10.0° for the components A and B, respectively. This criteria is employed because of weak remanence and a little instability of magnetic behavior of the component B. The samples whose direction of the component A deviated more than 20° from the site-mean direction were rejected regarding as artifact

21

because of the high concentration of the directions of the component A (described later). Such rejected sample was only one within site. The site-mean directions were re-calculated without the rejected samples, and the formation-mean directions were calculated using the site-mean directions averaged on three or more samples.

The site-mean directions and the formation-mean directions of the components A and B are summarized in Table 3 and 4, respectively. Either component of all samples showed normal polarity without exception. The directions of the component A made small clusters within site (Fig. 21). The 95% confidence limits of site-mean directions are all less than 15°. Site-mean directions also clustered well between sites, especially in geographic coordinate. The precision parameters (k_1 for geographic coordinate and k_2 for stratigraphic coordinate) are getting small after tilt-correction (k_2/k_1=0.44, 0.61 and 0.82 for the Hasandong Formation in Jinju area, the Hasandong Formation in Goreong area, the Chilgok and the Shilla Formations in Jinju area, respectively [McElhinny, 1964]).

The directions of the component B are scattered even within site (Fig. 22). The 95% confidence limits of site-mean directions are greater than 10° in many sites (Table 4). Although the directions are scattered, the site-mean directions and formation-mean direction directions of the Hasandong Formation in Jinju area are distinguishable from the component A. The declinations are similar to the component A, but the inclinations are shallower both before and after the tilt-correction (Fig. 22a and 23). The magnitudes of this shallowing are variable from sample to sample even within site. The directions of the component B seem to be distributed not as Fisher distribution but as fan-shape distribution where

the pivot is close to the mean direction of the component A (Fig. 23). On the other hand, site-mean directions of the component B of the Chilgok and the Shilla Formations are not distinguishable from the component A (Fig. 21c and 22b).

Non-red sedimentary rocks

The directions of the magnetite (maghemite) component for non-red samples are summarized in Table 5 and Fig. 24. Although the precision parameter (k) increases a very little after tilt-correction ($k_2/k_1=1.07$), the mean directions are very similar to that of the component A of red beds.

Discussion

Origin of the NRM components

Component A of red beds (Possibility of remagnetization and its acquisition timing)

All directions of the component A are of normal polarity. They are much concentrated either within site or between sites. Formation-mean directions also show better clustering between formations and between localities. Such high concentration seems to be unrealistic for DRM of older sedimentary rocks. After tilt correction, the directions are slightly scattered. Applied the fold test replacing k_2/k_1 to k_1/k_2, it is accepted at 95% significance that the observed magnetization was acquired after tilting only in the case of the Hasandong Formation in Jinju area [McElhinny, 1964]. Although this test is statistically negative in other cases, it is not significant because of homoclinal attitude of those sedimentary rocks. The precision parameters decrease in all cases after tilt-correction ($k_2/k_1 < 1$). This fact strongly suggests that the component A was acquired after tilting. The mean direction of the component A of only red beds is $D = 11.8°$, $I = 56.9°$ and $\alpha_{95} = 5.3°$ before tilt-correction (Table 3). This is distinguishable both from the present geomagnetic field direction ($D = -7°$, $I = 50°$) and the geocentric axial dipole field direction ($D = 0°$, $I = 55°$) at sampling area at 95% confidence level (Fig. 25). It is suggested that the component A was probably acquired secondarily but not in recent time.

The component A of red beds is carried not only by magnetite but also by hematite. Especially, that of the Hasandong Formation is carried mainly by hematite. The thermo-viscous origin of such component is unlikely because the maximum unblocking temperature (~640°C) is too high for the viscous magnetization acquired at low temperature [Pullaiah et al., 1975; Dunlop and Stirling, 1977].

The origin of NRM of red beds are controversial whether they are DRM or CRM [e.g. Roy and Park, 1972]. The hematite grains of chemical origin are generally smaller than those of detrital origin, because authigenic hematite grows slowly through the size of blocking volume [Channell et al., 1982]. Further, unblocking temperature of hematite is primarily a function of grain size [Néel, 1949]. The hematite grains with lower unblocking temperature are probably smaller. Therefore, it is thought that the low-temperature unblocking hematite is authigenic and carries CRM.

The strongly overprinted magnetizations in the Korean Peninsula have been reported not only from the Cretaceous rocks [Lee et al., 1987] but also from the pre-Cretaceous (Cambrian to Jurassic) rocks so far [Otofuji et al., 1986; Shibuya et al., 1988; Otofuji et al., 1989; Doh and Piper, 1994; Lee et al., 1996]. They are all of normal polarity and yields the similar pole positions each other. Therefore, the widespread remagnetization was thought to had occurred contemporaneously. Two ages have been proposed as the acquisition timing of this normal secondary remagnetization. One is at the Cretaceous Normal Superchron (118~83 Ma; Cande and Kent [1995]) [Shibuya et al., 1988; Doh and Piper, 1994], and the other is in recent time (Brunhes Normal Chron (0.78 Ma~; Cande and Kent [1995]) [Otofuji et al., 1986; Lee et al., 1987;

25

Otofuji et al., 1989]. Both are primarily based on the paleopole position and the polarity. It is not easy to speculate the timing of remagnetization simply based on paleomagnetic pole position, even if the Korean Peninsula firmly fixed to the main part of the eastern Asia. An accurate result is required because the pole positions from the neighborhood (China) since the Cretaceous time is not largely deviated from the recent one [Enkin et al., 1992].

Based on the normal polarity, magnetization acquisition timing requires rapid remagnetization or remagnetization in long normal chron. Authigenic hematite which grows slowly during diagenesis records the geomagnetic field direction when the size of hematite grains exceeds the critical volume [Channell et al., 1982]. The rapid remagnetization was unlikely to occur contemporaneously in the wide area without the corresponding geological evidence. Remagnetization in long normal chron, such as the Cretaceous Normal Superchron, is more plausible.

The most remarkable geological events which may have caused the Cretaceous remagnetization are the Bulguksa Disturbance. In the end of the Cretaceous time, the volcanic activity and the plutonic activity occurred in the Korean Peninsula, especially in southern part of the peninsula. It is highly possible that the secondary magnetization of the Gyeongsang Basin acquired at the time of the Bulguksa Disturbance. This event shared time with the Cretaceous Normal Superchron, because the age of granite which intruded at the Bulguksa Disturbance is about 115 Ma to 68 Ma [Lee (ed.), 1987].

It has been reported that the widespread remagnetization event might have occurred in the margin of Eastern Asia (Korea and Japan) at pre-Oligocene age [Moreau et al., 1987]. Since the late Mesozoic, this

26

region has been the continental margin in front of active subduction zone [Maruyama et al., 1997]. The eastern marginal area might have the similar condition that was suitable for the widespread remagnetization.

Component B of red beds (Reliability as the primary paleomagnetic directions)

The most samples from the Hasandong Formation at Jinju area yielded the component B. Many samples showed that these directions are clearly distinguishable from those of the component A. This is carried by the hematite with higher unblocking temperature and with lower coercivity.

The relationship between coercivity and grain size of hematite has not been well-determined [Dekkers and Linssen, 1989]. This is a function of crystalline anisotropy, and also influenced by the defects in the crystal lattice [Dunlop, 1970]. In some studies of red sediments, it was pointed out that the coercivity of the larger-grained hematite, including detrital origin, is lower than that of fine-grained hematite of chemical origin [Brooks and O'Reilly, 1970; Channell et al., 1982; Jackson and Van der Voo, 1986]. Combining the higher unblocking temperature range with this interpretation, it is concluded that the component B was carried by the larger hematite grains, possibly of detrital origin and carrying DRM. Those DRM is expected to be acquired before tilting.

The directions of the component B are scattered even within site, but they have a conspicuous feature. The distribution of the directions on the equal area projection fans out from the pivot around the direction of

27

the component A (Fig. 23). Compared with the directions of the component A, the direction of the component B has similar or shallower inclination (Fig. 26a, 26b and 26c). The declination is not largely different (Fig. 26d, 26e and 26f). What do these features mean and what causes the direction of the component B? Three conceivable hypothesis are given as follows, and are discussed about their plausibility.

Hypothesis 1: Large tectonic northward translation of the Korean Peninsula

First, simple hypothesis is that the direction of the component B correctly reflects the Cretaceous paleomagnetic direction. According to this hypothesis, Korea was located at lower latitude in the early Cretaceous time and moved northward to similar latitude as the present time by late Cretaceous. Using the site-mean direction (site JH010) and the sample direction (JH0134) of the components A and B tentatively, the maximum distance of northward translation is calculated $23 \pm 16°$ and $33°$ for latitude (2500 ± 1800 km and 3600 km), respectively.

Previous paleomagnetic studies on the pre-Cretaceous rocks reported that the southern part of the Korean Peninsula was located south compared to the present position by the Triassic [Shibuya et al., 1988; Doh and Piper, 1994], and moved northward by the Jurassic [Kim and Van der Voo, 1990; Lee et al., 1997]. Further, tectonic blocks of the main part of the eastern Asia (the North China Block and the Yangtze Block) almost combined into one unit and was located in close latitude similar to the present time in the Cretaceous [e.g. Enkin et al., 1992]. Their paleomagnetic pole position was almost stationary during the Cretaceous time. If the southern part of the Korean Peninsula was located

28

in low latitude in the early Cretaceous, only Korea drifted northward rapidly and collided to the main part of the eastern Asia during the Cretaceous. However, it is unlikely that the Korea migrated northwards rapidly between the time of DRM acquisition (early Cretaceous) and CRM acquisition (middle to late Cretaceous). This was not supported by both the geological and the geophysical evidence, such as tectonic sutures suggesting the tectonic collision since the Cretaceous time [Lee, 1987]. Although small northward movement cannot be ruled out, the large and rapid northward translation is implausible for the Korean Peninsula.

Hypothesis 2: Inseparable DRM from CRM with thermal demagnetization

The second hypothesis is that the direction of the component B was resultant direction of the primary and secondary components. This hypothesis means that the thermal demagnetization cannot separate these two directions completely and that true Cretaceous paleomagnetic direction is veiled.

The overlapping unblocking temperature spectra of two components with different directions mislead the estimation of the direction of the component B. In this case, curved trajectory on the orthogonal vector diagram is expected to be observed [Dunlop, 1979]. However, if two spectra overlap completely in constant proportion, linear magnetic component could be observed and the obtained direction would be intermediate between two [Dinarès-Turell and McClelland, 1991; Halim et al., 1996]. True direction is possibly obtainable by applying great circle method [Halls, 1976; McFadden and McElhinny, 1988]. But the application of such method is ineffective in this study, because the secondary component is so strong that obtained 'true' direction is just

reversed for the direction of the component A. It is strange that all magnetization are reversed, because the age of sedimentation corresponds to the mixed polarity chron of M-series before the Cretaceous Normal Superchron [Harland et al., 1990]. From this point of view, the component B may be also strange that they all are of normal polarity.

Roy and Park [1972] pointed out that DRM and CRM of red beds could not be completely separated only using thermal demagnetization. Lee et al. [1996], however, claimed that careful and detailed thermal demagnetization enabled to distinguish DRM and CRM. Lee et al. [1987] admitted that thermal demagnetization was possibly insufficient to separate the primary component from the remagnetization component for their paleomagnetic results from the Gyeongsang Basin. They invoked that the directions of reversed polarity had much shallower inclinations. As direction of reversed polarity is easier to distinguish from the secondary direction of normal polarity, the primary directions of reversed polarity may be more reliable. The direction of normal polarity is difficult to distinguish from the overprinted similar direction of normal polarity. The inappropriate separation of two directions of normal polarity may mislead them to find wrong primary directions in spite of their detailed demagnetization.

Inclination of the component B is likely to be shallower when low-field susceptibility is higher (Fig. 27). This suggests that low-field susceptibility reflects the amount of the low-coercivity hematite, because the component B is carried by the low-coercivity hematite. Few magnetite is contaminated in the samples as shown by thermomagnetic experiments. When low-coercivity hematite is less contained in the samples, low-field susceptibility is small and observed the component B is

probably covered or contaminated by the component A. Therefore, the second hypothesis is reasonable. The fan-shaped distribution of the component B also supports this hypothesis.

Hypothesis 3: Inclination shallowing of DRM due to compaction

The last hypothesis is that the direction of the component B was distorted by compaction after sedimentation. As the component B is carried by detrital hematite, it is possible to be suffered by the progressive compaction. The paleomagnetic direction after the compaction process is expected that inclination could be a little shallower than that of ancient geomagnetic field, but that declination cannot be largely changed except for small disturbance. The shallowing degree of inclination is thought to depend on the lithology and pressure [e.g. Sun and Kodama, 1992]. Inclination shallowing of red beds has been reported by several authors [Hodych and Buchan, 1994; Bazhenov et al., 1995; Stamatakos et al., 1995; Garcés et al., 1996]. However, the inclination shallowing of hematite grains is not well understood as magnetite grains [e.g. Jackson, 1991].

The compaction effects can well explain the observed dispersion of the directions of the component B. The resultant NRM direction was shifted to reduce its inclination by the stepwise thermal demagnetization, but downward direction never changed to upward one except for one sample with the inclination of nearly equal zero (Fig. 23). Although directions were apparently much scattered, the distribution of declinations did not largely deviated (Fig. 26d, 26e and 26f). These properties are coincides with the report by Tauxe et al. [1984].

31

The AMS degree is correlated with low-field susceptibility (Fig. 28), and its degree is small compared with the anisotropy of IRM (Table 2). As low-field susceptibility depends on the amount of low-coercivity hematite, such low degree of AMS is interpreted that abundant paramagnetic minerals of isotropic and low susceptibility reduce the AMS of anisotropy of hematite grains [Fuller, 1963]. AMS degree, in this case, does not represent the strength of alignment of hematite grains in samples due to compaction. AMS only suggests that the ferrimagnetic minerals in the sample is likely to be arranged more anisotropically than the observed AMS degree. Such a strong anisotropy not only of susceptibility but also of remanence cannot be ignored on assessment of the inclination shallowing of DRM direction.

According to the hypothesis of inclination shallowing, the early Cretaceous paleomagnetic direction should be steeper than the observed directions of the component B. The primary component expected to have similar inclination to that of the component A.

As discussed above, both hypothesis 2 and 3 are acceptable as the interpretation for the component B in this study. However they are not alternative. Only one hypothesis is insufficient for consistent explanation and therefore both hypotheses are required. Although some sample seems to yielded the component B clearly, it was not enough to say that they were not affected against the compaction process. The remagnetization is so strong that it is difficult to eliminate the overprinted component completely from NRM. This uncertainty does not allow us to correct the shallowed inclination to the original inclination using its anisotropy

degree such as the previous reports [Kodama and Davi, 1995; Garcés et al., 1996; Kodama, 1997].

The obtained component B does not represent the early Cretaceous paleomagnetic direction. The inclination might be disturbed strongly both by hypothesis 2 and 3, but the declination could be acceptable. The declinations are expected to scatter randomly during the post-depositional compaction, because of the oblate AMS fabric. The mean of the declination, therefore, represents the declination of primary direction at the time of deposition [Tauxe and Kent, 1984]. Although the declination might be affected by the component A due to the incomplete separation, the declination of the component B deflected a little easterly relative to the component A (Fig. 26a, 26b and 26c). As shown in Fig. 26a and 26b, this is not due to the tilt-correction. Easterly declination of the component B relative to that of the component A may reflect the difference of the paleomagnetic directions of the Korean Peninsula between the early Cretaceous and the middle to late Cretaceous.

Interpretation for the component of magnetite (maghemite)

In the studied area, magnetite has the same paleomagnetic direction as the secondary component of hematite in both red beds and non-red sedimentary rocks. The component carried by magnetite in red beds is indistinguishable from that carried by hematite of low unblocking temperature, and the mean direction from the non-red sediments is well consistent with the component A of red beds.

The origin of the magnetization of magnetite is not thermo-viscous remanence because of the same reason as hematite. The reversed component which observed in only one sample is likely to be thermo-viscous due to the very low unblocking temperature (~350°C). If the magnetite grains was primarily contributed to DRM, only the depositional hematite would be selectively suffered by compaction effect, and magnetic direction would not be changed largely in the interval between the acquisition of the DRM and CRM. The selective inclination shallowing might occur, considered with the structure of tabular hematite and cubic magnetite [Tauxe and Kent, 1984]. Another possibility is that not only low-temperature hematite but also magnetite has been remagnetized chemically in the study area, but magnetite and hematite does not grow simultaneously in the same condition.

Comparison with paleomagnetic poles in the vicinity of Korea and tectonic implications

It is suggested that the component A of red beds was acquired secondarily during the Cretaceous Normal Superchron. The direction of this component may be useful as the reliable paleomagnetic direction of the middle to late Cretaceous in the southern part of Korean Peninsula. The pole positions of the component A and the Cretaceous pole positions from China and the Southwest Japan are listed in Table 6 and shown in Fig. 29. The paleopole of the component A is overlapped completely with the late Cretaceous paleopoles from China [Enkin et al., 1992] (Fig. 29). It has been reported that the main part of the eastern Asia (the North

34

China Block and the Yangtze Block) had been combined at the Cretaceous time [e.g. Enkin et al., 1992]. Good agreement of these pole positions suggests that the Korean Peninsula was also combined to the main part of the eastern Asia in the Cretaceous time and did not move largely relative to China since that time.

The most remarkable tectonic event around Korea since the Cretaceous age was the opening of the Japan Sea [e.g. Otofuji, 1996]. The Japan arc was torn off from the vicinity of the Korean Peninsula and drifted rapidly from the Asian continent at the Miocene. The paleopoles from the Southwest Japan are largely deviated from the Cretaceous poles from Korea and China [Otofuji and Matsuda, 1987] (Fig. 29). The Southwest Japan was located beside the Korean Peninsula, especially the Gyeongsang Basin, before the Japan Sea opening. Nevertheless, the Gyeongsang Basin was never moved tectonically and had been stuck to the main part persistently against this event. This surprising stability of the Korean Peninsula was explained by the difference between the character of the lithosphere beneath the Korean Peninsula and the Japan arc [Otofuji et al., 1983].

Conclusions

Two magnetic components were observed from the red beds of the Gyeongsang Basin. The component A is carried by low-unblocking temperature hematite and/or magnetite and the component B is carried by high-unblocking temperature hematite. Based on the detailed rock magnetic analysis, the magnetic properties of hematite in red beds from the Gyeongsang Basin have following characteristics:

(1)   Hematite has been magnetized at two phases as evidenced by the different NRM directions. Although they can be separated with the stepwise thermal demagnetization rather than AF demagnetization, complete separation is difficult.

(2)   Low-temperature (~640°C) unblocking hematite is likely to be fine grain. This is thought to be authigenic and carries CRM. These grains carry very stable magnetization of the component A.

(3)   Hematite with the unblocking temperature around 675°C has larger grain size and detrital origin, which carries the component B of DRM origin. These grains have lower coercivity than smaller grains. The NRM direction carried by this hematite was affected by the inclination shallowing due to compaction, evidenced by the magnetic anisotropy which strongly corresponds to the sedimentary fabric. Such bias on CRM prevents us from approaching the true DRM direction and also from evaluating the degree of inclination shallowing of DRM.

Magnetization carried by magnetite was obtained from both red beds and non-red sedimentary rocks. This yielded the same direction as

36

the component A of hematite, while it is not determined whether magnetite carry DRM or CRM.

The component A is secondary magnetization by CRM after tilting. Timing of magnetic acquisition is estimated at the Cretaceous Normal Superchron, corresponding to the early time of the Bulguksa Disturbance. Mean direction of the component A of red beds is $D=11.8°$, $I=56.9°$ and $\alpha_{95}=5.3°$, corresponding to a paleopole at 80.2°N, 201.5°E and $A_{95}=6.4°$. Comparison of this paleopole with the Cretaceous paleopoles from China suggests that the Korean Peninsula was not moved largely relative to the main part of the eastern Asia since the late Cretaceous.

Acknowledgments

References

Bazhenov, M.L., V.L. Klishevich and V.A. Tselmovich, Palaeomagnetism of Permian red beds from south Kazakhstan: DRM inclination error or CRM shallowed directions?, Geophys. J. Int., 120, 445-452, 1995

Brooks, P.J. and W. O'Reilly, Magnetic rotational hysteresis characteristics of red sandstones, Earth Planet. Sci. Lett., 9, 71-76, 1970

Butler, R.F., Paleomagnetizm, Blackwell Scientific Publications, Boston, pp.319, 1992

Cande, S.C. and D.V. Kent, Revised calibration of the geomagnetic polarity timescale for the Late Cretaceous and Cenozoic, J. Geophys. Res., 100, 6093-6095, 1995

Channell, J.E.T., R. Freeman, F. Heller and W. Lowrie, Timing of diagenetic haematite growth in red pelagic limestones from Gubbio (Italy), Earth Planet. Sci. Lett., 58, 189-201, 1982

Collinson, D.W., The role of pigment and specularite in the remanent magnetism of red sandstones, Geophys. J. R. astr. Soc., 38, 253-264, 1974

Dekkers, M.J., Magnetic properties of natural goethite - III. Magnetic behavior and properties of minerals originating from goethite dehydration during thermal demagnetization, Geophys. J. Int., 103, 233-250, 1990

Dekkers, M.J. and J.H. Linssen, Rockmagnetic properties of fine-grained natural low-temperature haematite with reference to remanence acquisition mechanisms in red beds, Geophys. J. Int., 99, 1-18, 1989

Dinarès-Turell, J. and E. McClelland, A cautionary tale for palaeomagnetists: A spurious apparent single component remanence due to overlap of blocking-temperature spectra of two components, Geophys. Res. Lett., 18, 1297-1300, 1991

Doh, S.-J. and J.D.A. Piper, Paleomagnetism of the (Upper Palaeozoic - Lower Mesozoic) Pyongan Supergroup, Korea: a Phanerozoic Linc with the North China Block, Geophys. J. Int., 117, 850-863, 1994

Dunlop, D.J., Hematite: Intrinsic and defevt ferromagnetism, Science, 169, 858-860, 1970

Dunlop, D.J., On the use of Zijderveld vector diagrams in multicomponent paleomagnetic studies, Phys. Earth Planet. Inter., 20, 12-24, 1979

Dunlop, D.J. and J.M. Stirling, 'Hard' viscous remanent magnetization (VRM) in fine grained hematite, Geophys. Res. Lett., 4, 163-166, 1977

Elston, D.P. and M.E. Purucker, Detrital magnetization in red beds of the Moenkopi Formation (Triassic), Gray Mountain, Arizona, J. Geophys. Res., 84, 1653-1665, 1979

Enkin, R.J., Z. Yang, Y. Chen and V. Courtillot, Paleomagnetic constraints on the geodynamic history of the major blocks of China from Permian to the present, J. Geophys. Res., 97, 13953-13989, 1992

Fisher, R.A., Dispersion on a sphere, Proc. R. Soc. London, Ser. A, 217, 295-305, 1953

Fuller, M.D., Magnetic anisotropy and paleomagnetism, J. Geophys. Res., 68, 293-309, 1963

Garcés, M., J.M. Parés and L. Cabrera, Further evidence for inclination shallowing in redbeds, Geophys. Res. Lett., 23, 2065-2068, 1996

Halim, N., J.P. Cogné , V. Courtillot and Y. Chen, Apparent synfolding magnetization as a result of overlap of pre- and post-folding magnetizations, Geophys. Res. Lett., 23, 3523-3526, 1996

Halls, H.C., A least-squares method to find a remanence direction from converging remagnetization circles, Geophys. J. R. astr. Soc., 45, 297-304, 1976

Harland, W.B., R.L. Armstrong, A.V. Cox, L.E. Craig, A.G. Smith and D.G. Smith, A geologic time scale 1989, Cambridge University Press, Cambridge, pp.131, 1990

Hodych, J.P. and K.L. Buchan, Early Silurian palaeolatitude of the Springdale Group redbeds of central Newfoundland: a palaeomagnetic determination with a remanence anisotropy test for inclination error, Geophys. J. Int., 117, 640-652, 1994

Hodych, J.P., R.R. Pätzold and K.L. Buchan, Chemical remanent magnetization due to deep-burial diagenesis in oolitic hematite-bearing ironstones of Arabama, Phys. Earth Planet. Inter., 37, 261-284, 1985

IAGA Division V, Working Group 8, International Geomagnetic Reference Field, 1995 revision, J. Geomag. Geoelectr., 47, 1257-1261, 1995

Ito, H. and K. Tokieda, An interpretation of paleomagnetic results from Cretaceous Granites in South Korea, J. Geomag. Geoelectr., 32, 275-284, 1980

Jackson, M., Anisotropy of magnetic remanence: a brief review of mineralogical sources, physical origins, and geological applications,

and comparison with susceptibility anisotropy, Pure Appl. Geophys., 136, 1-28, 1991

Jackson, M. and R. Van der Voo, Thermaly activated viscous remanence in some magnetite- and hematite-bearing dolomite, Geophys. Res. Lett., 13, 1434-1437, 1986

Kienzle, J. and L.R. Scharon, Paleomagnetic comparison of Cretaseous rocks from South Korea and Late Paleozoic and Mesozoic rocks of Japan, Geophys. J. R. astr. Soc., 18, 413-416, 1966

Kim, K.H. and R. Van der Voo, Jurassic and Triassic paleomagnetism of South Korea, Tectonics, 9, 699-717, 1990

Kirschvinc, J.L., The least-squares line and plane and the analysis of paleomagnetic data, Geophys. J. R. astr. Soc., 62, 699-718, 1980

Kodama, K.P., A successful rock magnetic technique for correcting paleomagnetic inclination shallowing: Case study of the Nacimiento Formation, New Mexico, J. Geophys. Res., 102, 5193-5205, 1997

Kodama, K.P. and J.M. Davi, A compaction correction for the paleomagnetism of the Cretaceous Pigeon Point Formation of California, Tectonics, 14, 1153-1164, 1995

Lee, D.-S. (ed.), Geology of Korea, Kyohak-Sa, Seoul, pp.514, 1987

Lee, G., J. Besse, V. Courtillot and R. Montigny, Eastern Asia in the Cretaceous: new paleomagnetic data from south Korea and a new look at Chinese and Japanese data, J. Geophys. Res., 92, 3580-3596, 1987

Lee, Y.S., S. Nishimura and K.D. Min, High-unblocking-temperature haematite magnetizations of Late Palaeozoic red beds from the Okcheon zone, southern part of the Korean Peninsula, Geophys. J. Int., 125, 266-284, 1996

Lee, Y.S., S. Nishimura and K.D. Min, Paleomagnetotectonics of East Asia in the Proto-Tethys Ocean, Tectonophys., 270, 157-166, 1997

Løvlie, R. and T. Torsvik, Magnetic remanence and fabric properties of laboratory-deposited hematite-bearing red sandstone, Geophys. Res. Lett., 11, 229-232, 1984

Maruyama, S., Y. Isozaki, G. Kimura and M. Terabayashi, Paleogeographic maps of the Japanese Islands: Plate tectonic synthesis from 750 Ma to the present, The Island Arc, 6, 121-142, 1997

McElhinny, M.W., Statistical significance of the fold test in paleomagnetism, Geophys. J. R. astr. Soc., 8, 338-340, 1964

McFadden, P.L. and M.W. McElhinny, The combined analysis of remagnetization circles and direct observations in paleomagnetism, Earth Planet. Sci. Lett., 87, 161-172, 1988

Moreau, M.G., V. Courtillot and J. Besse, On the possibility of a widespread remagnetization of pre-Oligocene rocks from Northeast Japan and the Miocene rotational opening of the Japan Sea, Earth Planet. Sci. Lett., 84, 321-338, 1987

Nagata, T., K. Kobayashi and M.D. Fuller, Identification of magnetite and hematite in rocks by magnetic observation at low temperature, J. Geophys. Res., 69, 2111-2120, 1964

Néel, L., Théorie du trainage magnétique des ferromagnétiques en grains fins avec application aux terres cuites, Ann. Geophys., 5, 99-136, 1949

Otofuji, Y., Large tectonic movement of the Japan Arc in late Cenozoic times inferred from paleomagnetism: Review and synthesis, The Island Arc, 5, 229-249, 1996

Otofuji, Y., K. Katsuragi, H. Inokuchi, K. Yaskawa, K.H. Min, D.S. Lee and H.Y. Lee, Remagnetization of Cambrian to Triassic sedimentary rocks of the Paegunsan Syncline of the Okch'on Zone, South Korea, J. Geomag. Geoelectr., 41, 119-135, 1989

Otofuji, Y., K.H. Kim, H. Inokuchi, H. Morinaga, F. Murata, H. Katao and K. Yaskawa, A paleomagnetic reconnaissance of Permian to Cretaceous sedimentary rocks in southern part of Korean Peninsula, J. Geomag. Geoelectr., 38, 387-402, 1986

Otofuji, Y. and T. Matsuda, Amount of clockwise rotation of Southwest Japan - fan shape opening of the soithwestern part of the Japan Sea, Earth Planet. Sci. Lett., 85, 289-301, 1987

Otofuji, Y., J.Y. Oh, T. Hirajima, K.D. Min and S. Sasajima, Paleomagnetism and age determination of Cretaceous rocks from Gyeongsang Basin, Korean Peninsula, in The Tectonic and Geologic Evolution of Southeast Asian Seas and Islands: Part 2, Geophys. Monogr. Ser., vol.27, AGU, Washington, D.C., pp.388-396, 1983

Özdemir, Ö., D.J. Dunlop and B.M. Moskowitz, The effect of oxidation on the Verwey transition in magnetite, Geophys. Res. Lett., 20, 1671-1674, 1993

Pullaiah, G., E. Irving, K.L. Buchan and D.J. Dunlop, Magnetization changes caused by burial and uplift, Earth Planet. Sci. Lett., 28, 133-143, 1975

Rochette, P., G. Fillion, J.-L. Mattéi and M.J. Dekkers, Magnetic transition at 30-34 Kelvin in pyrrhotite: insight into a widespread occurence of this mineral in rocks, Earth Planet. Sci. Lett., 98, 319-328, 1990

Roy, J.L. and J.K. Park, Red beds: DRM or CRM?, Earth Planet. Sci. Lett., 17, 211-216, 1972

Shibuya, H., K.D. Min, Y.S. Lee, S. Sasajima and S. Nishimura, Paleomagnetismof Cambrian to Jurrasic sedimentary rocks from the Ogcheon Zone, southern part of Korean Peninsula, J. Geomag. Geoelectr., 40, 1469-1480, 1988

Stamatakos, J., A.M. Lessard, B.A.v.d. Pluijm and R.V.d. Voo, Paleomagnetism and magnetic fabrics from the Springdale and Wigwam Redbeds of Newfoundland and their implications for the Silurian paleolatitude controversy, Earth Planet. Sci. Lett., 132, 141-155, 1995

Steiner, M.B., Detrital remanent magnetization in hematite, J. Geophys. Res., 88, 6523-6539, 1983

Sun, W.W. and K.P. Kodama, Magnetic anisotropy, scanning electron microscopy, and X ray pole figure goniometry study of inclination shallowing in a compacting clay-rich sediment, J. Geophys. Res., 97, 19599-19615, 1992

Tarling, D.H. and F. Hrouda, The magnetic anisotropy of rocks, Chapman & Hall, London, pp.217, 1993

Tauxe, L., C. Constable, L. Stokking and C. Badgley, Use of anisotropy to determin the origin of characteristic remanence in the Siwalik red beds of northern Pakistan, J. Geophys. Res., 95, 4391-4404, 1990

Tauxe, L. and D.V. Kent, Properties of a detrital remanence carried by haematite from study of modern river deposits and laboratory redeposition experiments, Geophys. J. R. astr. Soc., 77, 543-561, 1984

Tauxe, L., D.V. Kent and N.D. Opdyke, Magnetic components contributing to the NRM of Middle Siwalik red beds, Earth Planet. Sci. Lett., 47, 279-284, 1980

Torii, M., K. Fukuma, C.-S. Horng and T.-Q. Lee, Magnetic discrimination of pyrrhotite- and greigite-bearing sediment samples, Geophys. Res. Lett., 23, 1813-1816, 1996

Turner, P., The palaeomagnetic evolution of continental red beds, Geol. Mag., 116, 289-301, 1979

van Velzen, A.J. and J.D.A. Zijderveld, A method to study alterlation of magnetic minerals during thermal demagnetization applied to a fine-grained marine marl (Trubi formation, Sicily), Geophys. J. Int., 110, 79-90, 1992

Zijderveld, J.D.A., A.C. demagnetization of rocks: Analysis of results, in Method in paleomagnetism, edited by D.W. Collinson, K.M. Creer and S.K. Runcorn, Elsevier, Amsterdam, pp.254-286, 1967

Table 1. Paleomagnetic sampling site.

site No.	N	location area	lat.(°N)	long.(°E)	formation	rock color	bedding attitude strike(°)	dip(°)
JH001	5	Jinju	35°15.4'	127°59.7'	Hasandong	red	3	18
JH002	5	Jinju			Hasandong	red	3	18
JH003	5	Jinju			Hasandong	red	3	18
JH004	5	Jinju			Hasandong	grey	3	18
JH006	5	Jinju	35°14.3'	128°00.1'	Hasandong	grey	6	8
JH007	5	Jinju	35°14.0'	128°00.3'	Hasandong	grey	-2	8
JH008	6	Jinju			Hasandong	red	8	7
JH009	3	Jinju			Hasandong	red	8	7
JH010	5	Jinju	35°13.2'	128°01.5'	Hasandong	red	-1	6
JH011	5	Jinju			Hasandong	red	-1	6
JH012	5	Jinju			Hasandong	red	-1	6
JH013	6	Jinju			Hasandong	red	-1	6
JH014	6	Jinju			Hasandong	red	25	5
JH015	5	Jinju			Hasandong	red	25	5
JH016	5	Jinju			Hasandong	red	25	5
JH017	5	Jinju	35°13.8'	127°59.4'	Hasandong	red	-15	13
JH018	5	Jinju			Hasandong	red	-15	13
JH019	5	Jinju			Hasandong	red	-15	13
JH020	5	Jinju	35°12.6'	128°02.0'	Hasandong	red	9	2
JH049	5	Jinju	35°11.1'	128°02.5'	Hasandong	red	14	10
JH050	5	Jinju			Hasandong	red	14	10
JH051	5	Jinju			Hasandong	red	13	8
JH052	5	Jinju			Hasandong	red	10	6
JJ039	5	Jinju	35°09.3'	128°07.3'	Jinju	grey	7	11
JJ040	5	Jinju			Jinju	grey	7	11
JJ041	5	Jinju			Jinju	grey	10	15
JJ042	5	Jinju			Jinju	grey	10	15
JJ043	5	Jinju			Jinju	grey	11	14
JJ044	5	Jinju			Jinju	grey	5	12
JJ045	5	Jinju	35°08.5'	128°06.3'	Jinju	grey	21	12
JJ046	5	Jinju			Jinju	grey	21	12
JJ047	5	Jinju	35°09.2'	128°04.1'	Jinju	grey	10	7
JJ048	5	Jinju			Jinju	grey	14	8
JC037	5	Jinju	35°09.8'	128°09.2'	Chilgok	red	-8	19
JC038	8	Jinju	35°09.8'	128°09.3'	Chilgok	red	39	10
JC151	8	Jinju	35°09.8'	128°10.0'	Chilgok	red	-7	8
JC152	8	Jinju	35°10.2'	128°10.7'	Chilgok	red	42	7
UC021	6	Jinju	35°15.7'	128°13.3'	Chilgok	red	45	7
UC022	5	Jinju			Chilgok	red	45	7
UC023	5	Jinju			Chilgok	red	45	7
UC024	5	Jinju			Chilgok	red	45	7
JS153	8	Jinju	35°10.2'	128°11.2'	Shilla	red	62	2
US025	5	Jinju	35°15.5'	128°13.7'	Shilla	red	43	2
US026	5	Jinju			Shilla	red	43	2
GH089	5	Goreong	35°42.9'	128°18.5'	Hasandong	red	18	20
GH091	5	Goreong	35°43.4'	128°17.4'	Hasandong	red	47	22
GH092	5	Goreong			Hasandong	red	35	21
GH093	5	Goreong			Hasandong	red	35	21
GH094	5	Goreong			Hasandong	red	40	17
GH095	5	Goreong			Hasandong	red	40	26
GH096	5	Goreong			Hasandong	red	40	23
GH097	5	Goreong			Hasandong	red	35	18
GH098	5	Goreong			Hasandong	red	34	20

N is number of collected samples.

Table 2. Anisotropy of IRM and anisotropy of low-field susceptibility.

Sample No.	Anisotropy of IRM				Anisotropy of susceptibility (AMS)		
	Inc. of IRMv	IRMv/IRMh			Inc. of K3	K3/K1	K3/K2
		(≤0.3T)	(0.3~1T)	(≥1T)			
JH0081	79°	0.841	0.736	0.933	86°	0.914	0.916
JH0135	87°	0.737	0.675	1.100	84°	0.938	0.940
JH0171	86°	0.932	0.918	0.964	81°	0.988	0.989

Direction of IRMv was defined arbitrarily, but that of K3 was caluculated for AMS fablic.

Table 3. Paleomagnetic results of the component A from redbeds; site-mean directions, formation-mean directions and their Fisher's statistics.

				In situ		Tilt corrected				
Site No.	area	formation	n / N	Dec.(°)	Inc.(°)	Dec.(°)	Inc.(°)	k	α95(°)	remarks
JH001	Jinju	Hasandong	4 / 5	11.9	61.2	38.7	54.1	470.6	4.2	
JH002	Jinju	Hasandong	2 / 2	10.9	60.6	37.6	53.9	(720.6	9.3)	*1
JH003	Jinju	Hasandong	4 / 4	14.8	61.1	40.7	53.4	119.9	8.4	
JH008	Jinju	Hasandong	6 / 6	9.6	55.8	19.7	55.0	234.9	4.4	
JH009	Jinju	Hasandong	3 / 3	8.2	61.6	20.9	60.8	174.5	9.4	
JH010	Jinju	Hasandong	5 / 5	11.6	56.8	20.2	55.1	99.4	7.7	
JH011	Jinju	Hasandong	5 / 5	14.3	56.5	22.6	54.5	282.0	4.6	
JH012	Jinju	Hasandong	1 / 2	29.5	66.7	39.9	63.1			*1
JH013	Jinju	Hasandong	6 / 6	14.7	58.1	23.4	56.0	153.1	5.4	
JH014	Jinju	Hasandong	4 / 5	11.2	51.4	17.4	52.4	50.2	13.1	
JH015	Jinju	Hasandong	5 / 5	10.6	59.2	19.0	60.1	48.0	11.2	
JH016	Jinju	Hasandong	3 / 4	10.9	58.0	18.9	58.8	127.4	11.0	
JH017	Jinju	Hasandong	5 / 5	15.6	63.3	32.6	54.9	228.3	5.1	
JH018	Jinju	Hasandong	4 / 5	16.8	57.3	30.5	49.1	266.8	5.6	
JH019	Jinju	Hasandong	5 / 5	6.1	58.0	22.3	51.5	297.1	4.4	
JH020	Jinju	Hasandong	3 / 3	11.1	57.9	14.2	57.8	589.0	5.1	
JH049	Jinju	Hasandong	5 / 5	21.0	54.7	34.3	52.4	133.6	6.6	
JH050	Jinju	Hasandong	5 / 5	18.2	53.9	31.3	52.1	177.4	5.8	
JH051	Jinju	Hasandong	5 / 5	18.3	58.0	30.5	56.4	221.8	5.1	
JH052	Jinju	Hasandong	5 / 5	15.0	59.1	24.7	58.1	255.2	4.8	
mean	Jinju	Hasandong	18 / 20	13.4	57.9			516.3	1.5	
						25.9	55.4	225.8	2.3	
UC021	Jinju	Chilgok	6 / 6	10.3	56.8	20.3	60.3	324.4	3.7	
UC022	Jinju	Chilgok	5 / 5	12.4	59.4	23.6	62.6	234.1	5.0	
UC023	Jinju	Chilgok	4 / 5	17.4	60.4	29.5	62.9	323.2	5.1	
UC024	Jinju	Chilgok	5 / 5	15.2	59.2	26.6	62.0	688.6	2.9	
JC037	Jinju	Chilgok	3 / 3	12.6	55.6	32.9	45.8	312.4	7.0	
JC038	Jinju	Chilgok	8 / 8	7.6	53.4	20.9	57.7	130.7	4.9	
JC151	Jinju	Chilgok	7 / 8	13.1	60.5	25.0	57.0	322.9	3.4	
JC152	Jinju	Chilgok	7 / 7	0.4	55.1	1.9	56.8	263.5	3.7	
US025	Jinju	Shilla	5 / 5	16.1	57.1	19.0	57.9	313.9	4.3	
US026	Jinju	Shilla	4 / 5	67.1	72.5	72.6	71.6	58.8	12.1	
JS153	Jinju	Shilla	6 / 6	9.0	56.4	-1.7	48.9	234.6	4.4	
mean	Jinju	Chilgok+Shilla	11 / 11	13.8	59.4			87.9	4.9	
						22.1	59.5	53.0	6.3	
GH089	Goreong	Hasandong	5 / 5	10.7	53.5	37.0	51.3	136.7	6.6	
GH091	Goreong	Hasandong	4 / 5	4.9	55.9	41.7	65.2	55.4	12.5	
GH092	Goreong	Hasandong	5 / 5	9.3	48.2	34.8	53.1	104.8	7.5	
GH093	Goreong	Hasandong	3 / 3	1.4	53.2	32.5	60.0	227.7	8.2	
GH094	Goreong	Hasandong	5 / 5	10.1	54.3	35.4	59.5	257.5	4.8	
GH095	Goreong	Hasandong	4 / 5	12.2	50.2	46.9	55.2	92.0	9.6	
GH096	Goreong	Hasandong	4 / 5	13.5	47.1	40.6	52.4	614.8	3.7	
GH097	Goreong	Hasandong	5 / 5	5.4	65.5	48.4	68.2	569.1	3.2	
GH098	Goreong	Hasandong	4 / 5	8.6	52.4	36.6	56.4	422.5	4.5	
mean	Goreong	Hasandong	9 / 9	8.7	53.4			191.9	3.7	
						39.0	58.0	157.1	4.1	
mean of formation-means of red b			3 / 3	11.8	56.9			536.5	5.3	
						29.0	57.8	249.5	7.8	

N is number of measured samples, and n is number of samples which used for the calculation of mean directions. *1 is not used for calculating formation mean.

49

Table 4. Paleomagnetic results of the component B from redbeds; site-mean directions, formation-mean directions and their Fisher's statistics.

Site No.	area	formation	n / N	In situ Dec.(°)	Inc.(°)	Tilt corrected Dec.(°)	Inc.(°)	k	α95(°)	remarks
JH001	Jinju	Hasandong	4 / 5	20.9	56.2	41.4	47.5	137.1	7.9	
JH002	Jinju	Hasandong	2 / 2	20.4	52.6	38.9	44.5	(210.3	17.3)	*1
JH003	Jinju	Hasandong	4 / 4	17.8	56.6	39.4	48.7	132.2	8.0	
JH008	Jinju	Hasandong	4 / 6	23.8	31.8	27.8	29.7	41.0	14.5	
JH009	Jinju	Hasandong	-							*2
JH010	Jinju	Hasandong	4 / 5	33.6	31.4	36.4	27.8	53.3	12.7	
JH011	Jinju	Hasandong	1 / 5	54.4	30.0	56.1	25.0			*1
JH012	Jinju	Hasandong	1 / 2	65.8	44.9	67.9	39.4			*1
JH013	Jinju	Hasandong	5 / 6	30.3	29.6	33.0	26.4	11.9	23.1	
JH014	Jinju	Hasandong	4 / 5	18.7	25.9	21.1	26.4	17.8	22.4	
JH015	Jinju	Hasandong	4 / 5	14.9	33.0	18.2	33.8	11.1	28.9	
JH016	Jinju	Hasandong	2 / 4	15.5	36.5	19.2	37.2	(128.6	22.2)	*1
JH017	Jinju	Hasandong	5 / 5	27.1	59.8	39.5	50.1	166.1	6.0	
JH018	Jinju	Hasandong	4 / 5	30.7	50.0	39.1	40.0	33.2	16.2	
JH019	Jinju	Hasandong	3 / 5	12.6	51.5	24.7	44.2	106.9	12.0	
JH020	Jinju	Hasandong	1 / 3	1.6	68.2	6.5	68.4			*1
JH049	Jinju	Hasandong	4 / 5	17.7	39.2	25.6	37.9	55.4	12.4	
JH050	Jinju	Hasandong	5 / 5	26.3	37.5	33.3	34.8	22.4	16.5	
JH051	Jinju	Hasandong	3 / 5	19.8	41.9	26.8	40.5	35.5	21.0	
JH052	Jinju	Hasandong	5 / 5	22.9	63.2	33.8	61.3	40.5	12.2	
mean	Jinju	Hasandong	14 / 19	22.8	43.6			36.9	6.6	
						31.0	39.4	47.2	5.8	
UC021	Jinju	Chilgok	4 / 6	7.1	54.7	15.9	58.6	21.8	20.1	
UC022	Jinju	Chilgok	4 / 5	8.3	54.4	17.2	58.2	52.9	12.8	
UC023	Jinju	Chilgok	3 / 5	15.9	65.8	31.4	68.4	86.6	13.3	
UC024	Jinju	Chilgok	0 / 5							
JC037	Jinju	Chilgok	2 / 3	22.7	55.2	40.0	43.0	(259.9	15.6)	*1
JC038	Jinju	Chilgok	4 / 8	11.6	53.9	25.5	57.5	45.5	13.8	
JC151	Jinju	Chilgok	-							*2
JC152	Jinju	Chilgok	-							*2
US025	Jinju	Shilla	0 / 5							
US026	Jinju	Shilla	4 / 5	76.1	71.9	80.9	70.7	72.9	10.8	
JS153	Jinju	Shilla	-							*2
mean	Jinju	Chilgok+Shilla	5 / 8	17.4	61.9			32.4	13.6	
						28.7	64.6	43.7	11.2	
GH089	Goreong	Hasandong	2 / 5	35.9	40.8	49.5	32.3	(36.3	42.7)	*1
GH091	Goreong	Hasandong	1 / 5	30.8	29.4	44.2	33.0			*1
GH092	Goreong	Hasandong	2 / 5	4.7	58.0	41.8	62.6	(40.2	40.5)	*1
GH093	Goreong	Hasandong	0 / 3							
GH094	Goreong	Hasandong	0 / 5							
GH095	Goreong	Hasandong	2 / 5	21.3	54.5	59.0	54.3	(71.3	30.0)	*1
GH096	Goreong	Hasandong	1 / 5	23.9	16.2	31.5	21.1			*1
GH097	Goreong	Hasandong	2 / 5	17.6	47.8	38.4	50.0	(8.9	97.2)	*1
GH098	Goreong	Hasandong	4 / 5	20.9	46.2	42.4	47.0	131.2	10.8	*1
mean	Goreong	Hasandong	0 / 7							

Samples of *2 were not measured above 640°C. Other details are same as Table3.

50

Table 5.　　　Site-mean and formation-mean directions of the Jinju Formation.

Site No.	area	formation	n / N	In situ		Tilt corrected		k	α95(°)	remarks
				Dec.(°)	Inc.(°)	Dec.(°)	Inc.(°)			
JJ039	Jinju	Jinju	3 / 3	20.5	58.8	36.2	54.8	78.8	14.0	
			1 / 3	184.7	-61.7	204.6	-60.3			(~350°C), *1
JJ041	Jinju	Jinju	3 / 3	5.4	57.5	28.3	55.7	247.1	7.9	
JJ042	Jinju	Jinju	3 / 3	11.8	56.7	33.0	53.5	202.5	8.7	
JJ044	Jinju	Jinju	3 / 3	18.4	60.4	36.4	55.7	315.0	7.0	
JJ045	Jinju	Jinju	2 / 3	10.4	54.5	27.5	55.0	(4331.3	3.8)	(~500°C), *1
JJ046	Jinju	Jinju	3 / 3	6.1	51.3	21.5	52.8	261.4	7.6	
JJ047	Jinju	Jinju	3 / 3	8.7	57.9	19.7	57.4	147.7	10.2	
JJ048	Jinju	Jinju	2 / 3	9.0	59.1	22.3	58.8	(112.7	23.7)	*1
mean	Jinju	Jinju	6 / 8	11.5	57.2			307.4	3.8	
						29.2	55.2	327.7	3.7	

Details are same as Table 3.

Table 6. Cretaceous paleomagnetic poles from the Gyeongsang Basin and its vicinity.

location	age	VGP lat.(°N)	long.(°E)	A95(°)	reference
Gyeongsang Basin	K2	80.2	201.5	6.4	This study (component A, in situ)
All China	K2	78.1	203.2	7.5	[Enkin et al., 1992]
All China	K1	78.1	216.8	5.5	[Enkin et al., 1992]
SW Japan	92-80Ma	28.0	210.0	9.8	[Otofuji and Matsuda, 1987]
SW Japan	112-85Ma	41.5	189.4	8.5	[Otofuji and Matsuda, 1987]

K1 and K2 is the early and the late Cretaceous, respectively. The poles from China were calculated using the poles without the poles from Korea, Shandong, Mongolia or Tarim blocks.
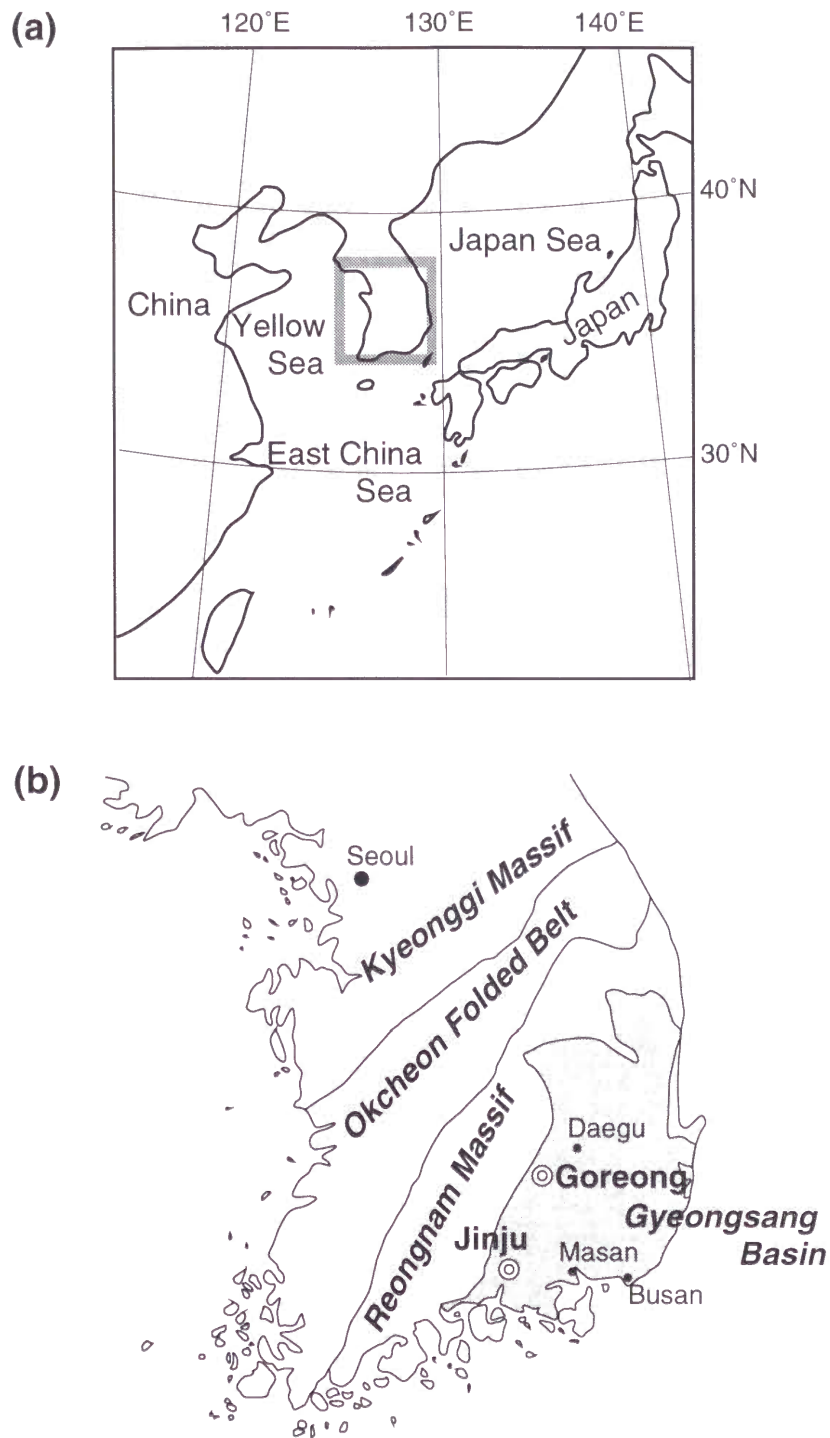
Figure 1. (a) Location of the Korean Peninsula. (b) Simplified tectonic map of the southern part of the Korean Peninsula. The shaded area is the Gyeongsang Basin where the Cretaceous sedimentary rocks are distributed. Sampling locations are shown by double circles.

Period	C N S	Supergroup	Group	Subdivision	Site code Jinju area	Goreong area
Paleogene						
Upper Cretaceous		(Bulgksa granite)				
			Yucheon G. (volcanic rocks)			
	?	Gyeongsang Supergroup	Hayang G.	Jindong F.		
	?			Haman F.		
Lower Cretaceous				Shilla F.	JS, US	
				Chilgok F.	JC, UC	
			Shindong G.	Jinju F.	JJ	
				Hasandong F.	JH	GH
				Naktong F.		
Jurassic		(Daebo granite)				

Figure 2. Generalized stratigraphy of the Cretaceous period in the southern Part of the Korean Peninsula, modified after Lee (ed.) [1987]. The subdivision of the Gyeongsang Supergroup are different for each locality. This classification is applied for the sampling region. Double lines indicate unconformity. CNS is the expected duration of Cretaceous Normal Superchron. The corresponding formation to its lower limit is unknown.

(a)

35°
20´N

0　5　10km

JH001-003
○JH004
JH006
○JH007
JH017-019
○JH008-009
●JH020
JH010-016　●
JH049-052　●

US021-024　●　US025-026

Namgang River

Jinju
◎

Masan

JC037-038　JC152
JC152
JS153
JJ039-044　○
JC151

JJ047-048　○
JJ045-046　○

Nakdong F.

Hasandong F.

Jinju F.

Chilgok F.

Shilla F.

Haman F.

Jindong F.

10´N

128°00´E　　10´　　35°

Alluvium

Cretaceous granites (Bulgugsa series)

Cretaceous andesite (Yuchon group)

Cretaceous sediments

Precambrian gneiss

55

(b)

35°
45´N

Goreong
◎

GH098
GH091
GH089

Jinju F.

Chilgok F.

Shilla F.

Haman F.

Hasandong F.

Naktong River

0　2　4km

128°15´E　　20´　　25´　　40´

Figure 3. (a) Geological map around Jinju. Solid and open circles denote the paleomagnetic sampling sites of red beds and non-red sedimentary rocks, respectively. (b) Simplified geological map and the sampling sites around Goreong.
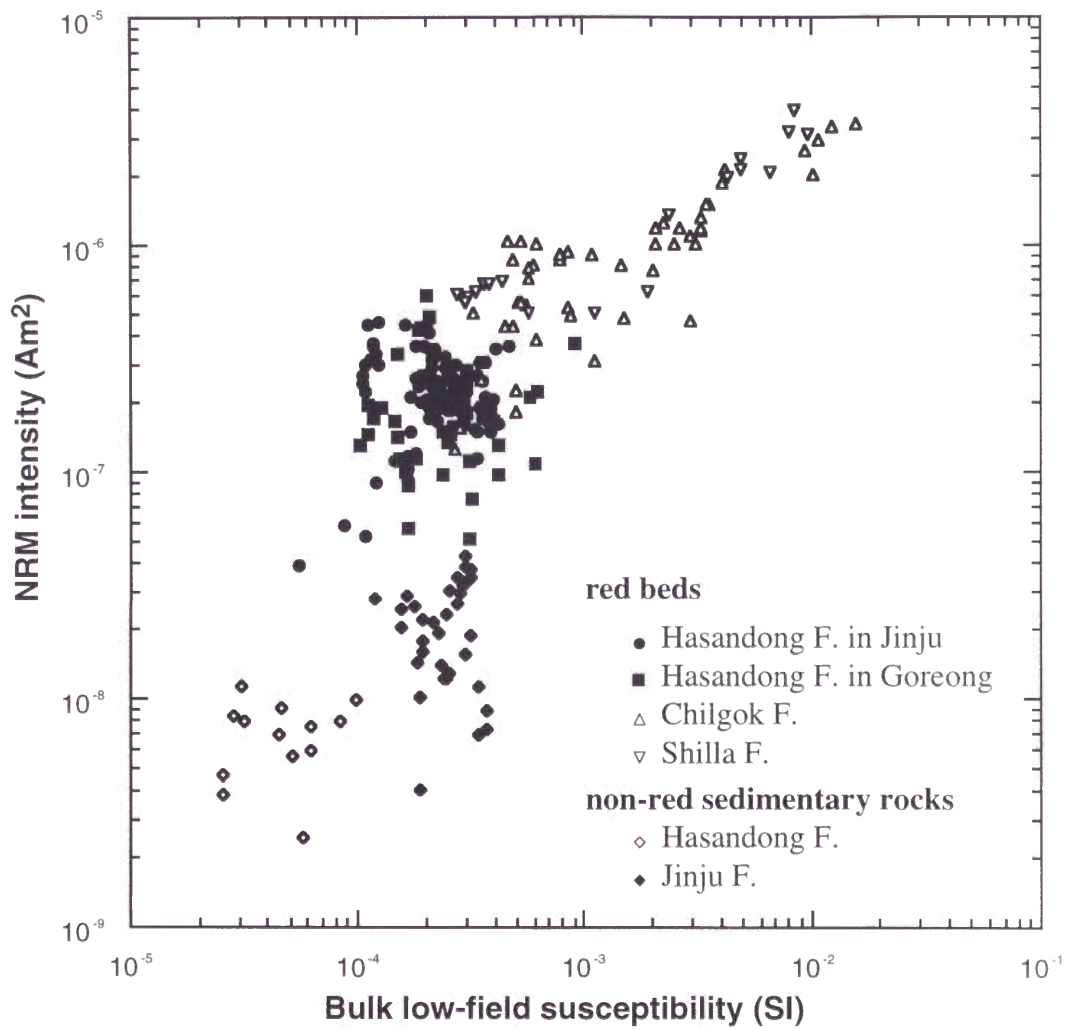
Figure 4. Intensity of natural remanent magnetization vs. low-field susceptibility of all measured samples.

(a) JH0033
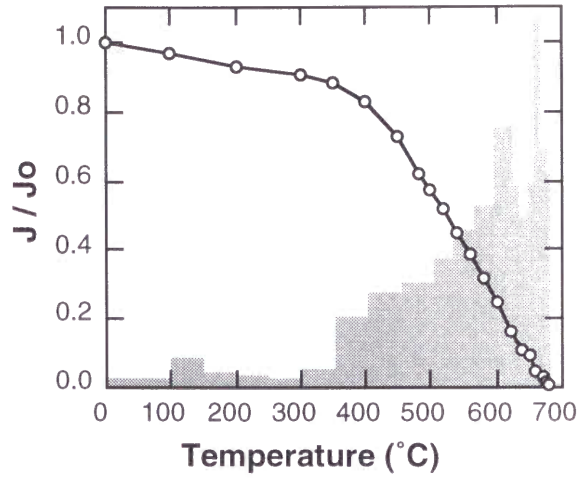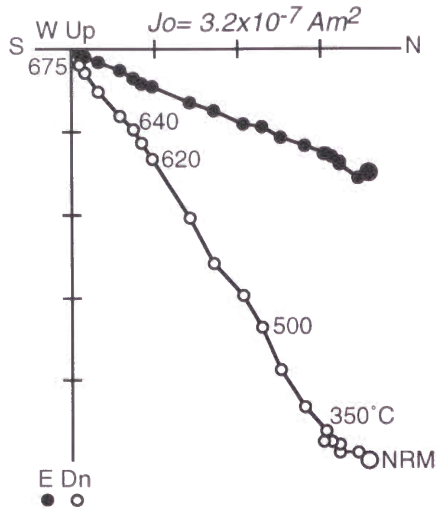
(b) JH0171
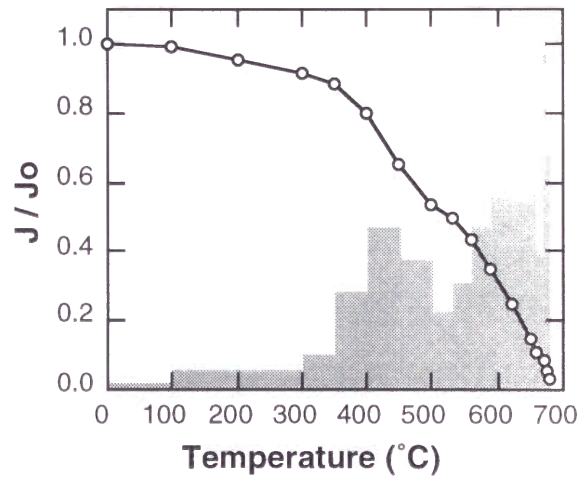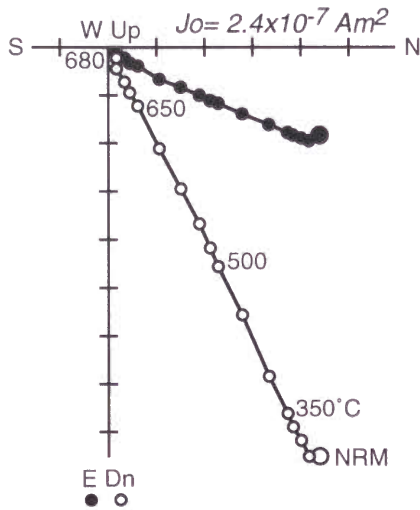
(c) JH0192
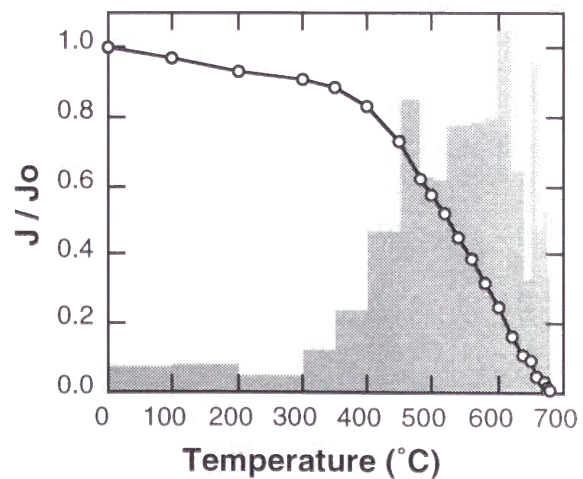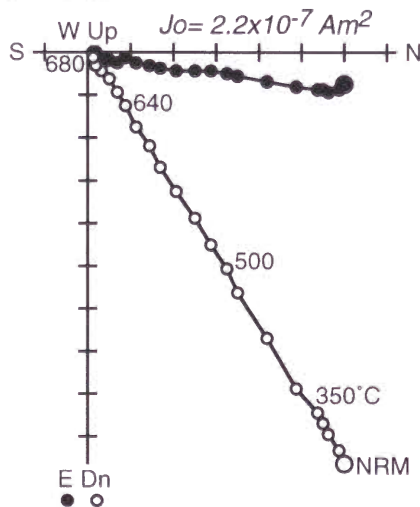
Figure 5. Results of representative samples of red beds from the Hasandong Formation in Jinju area during thermal demagnetization. (Left) Orthogonal projections of magnetization vector end points in geographic coordinate. Solid (open) circles are projected onto horizontal (vertical) planes. (Right) Intensity decay curves with unblocking temperature spectrum (gray bars in arbitrary scale).

(d) JH0135
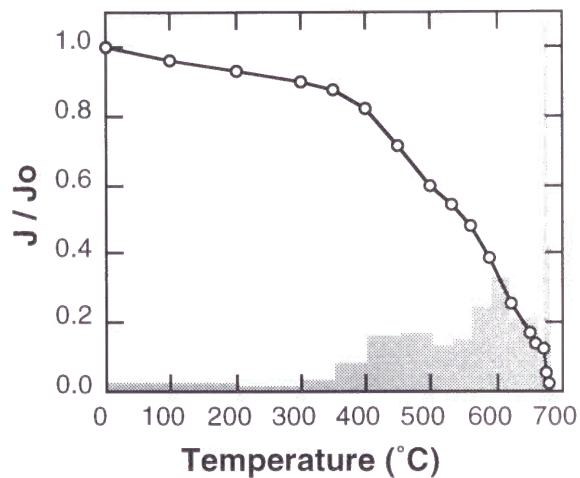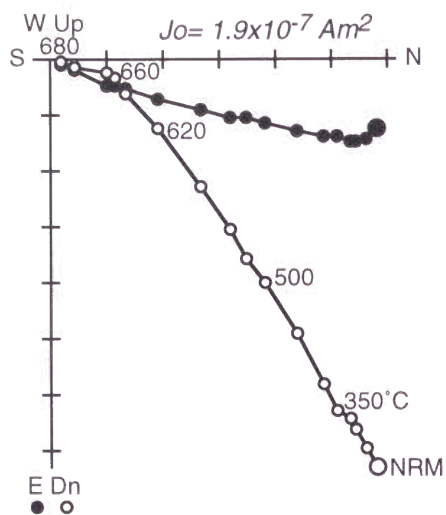
(e) JH0151
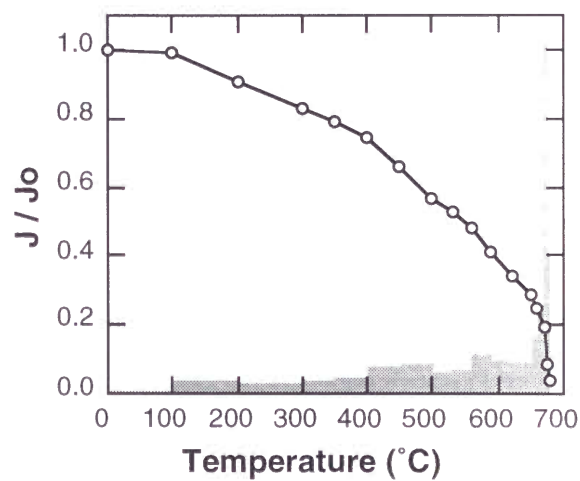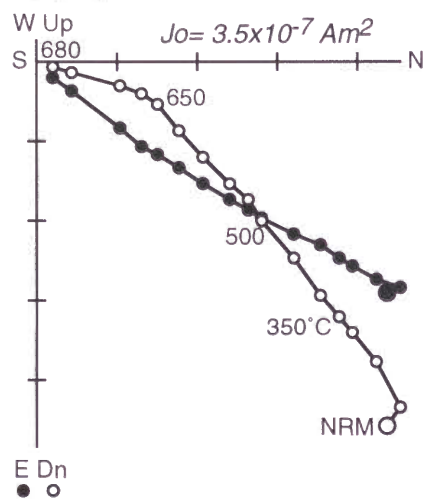
(f) JH0184
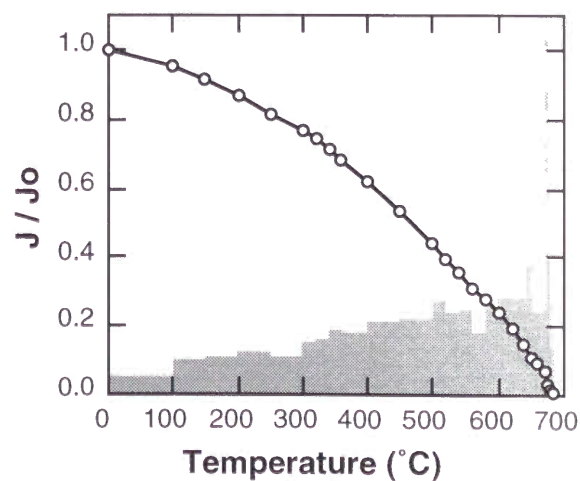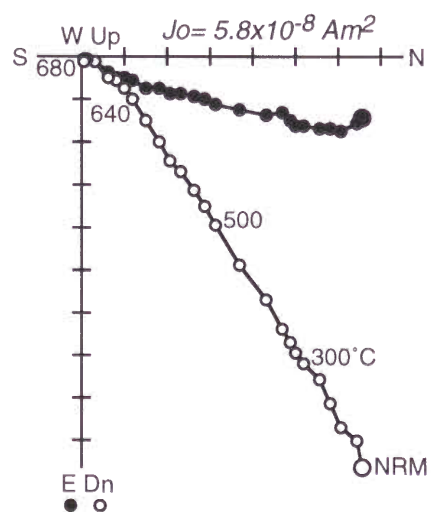
Figure 5. (continued)
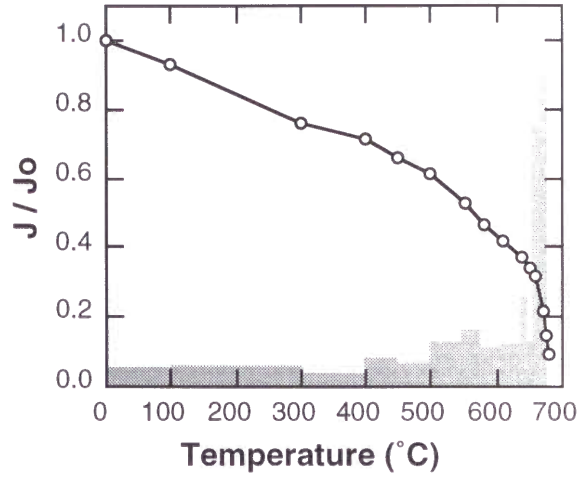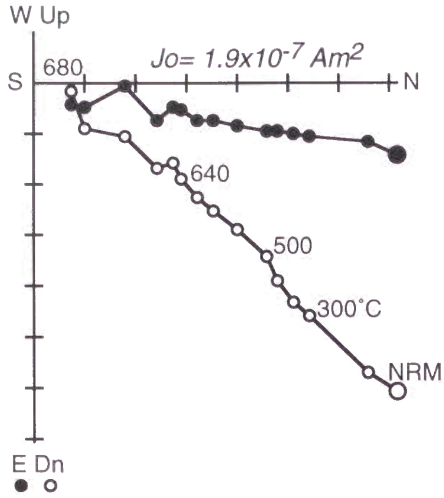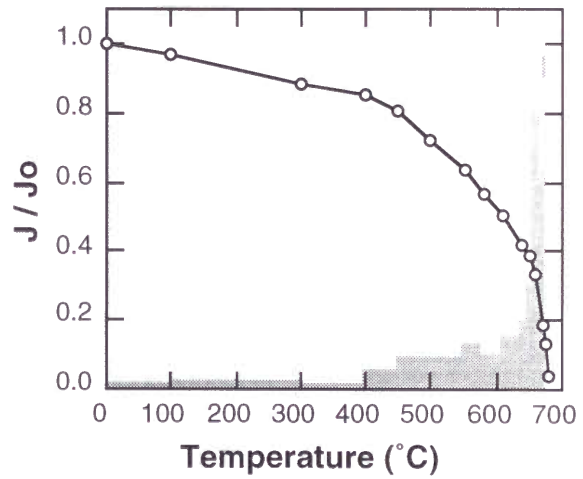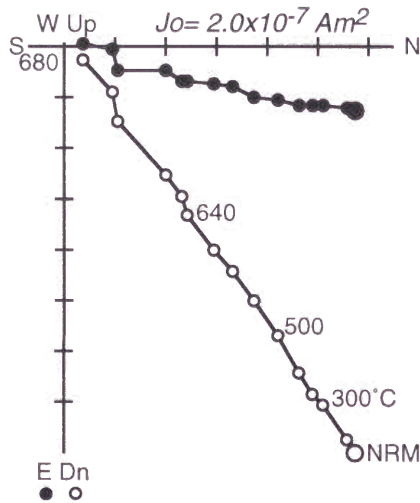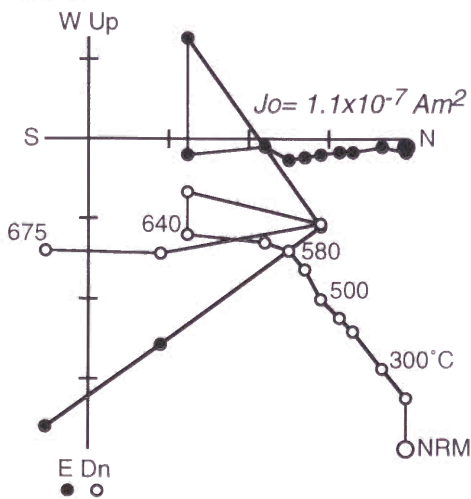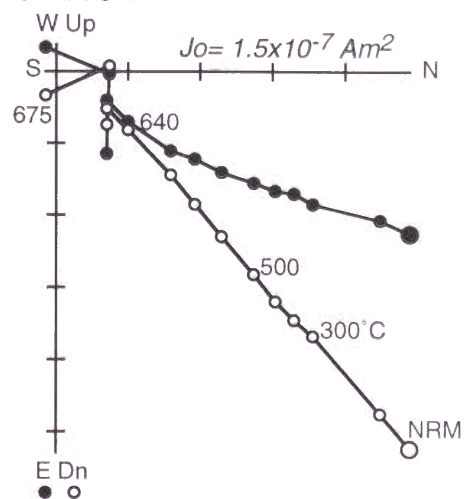
Figure 6. Results of representative samples of red beds from the Hasandong Formation in Goreong area during thermal demagnetization. Details are same as Fig. 5, except that (c) and (d) are without intensity decay curves.

59

(a)

(b)

(c)
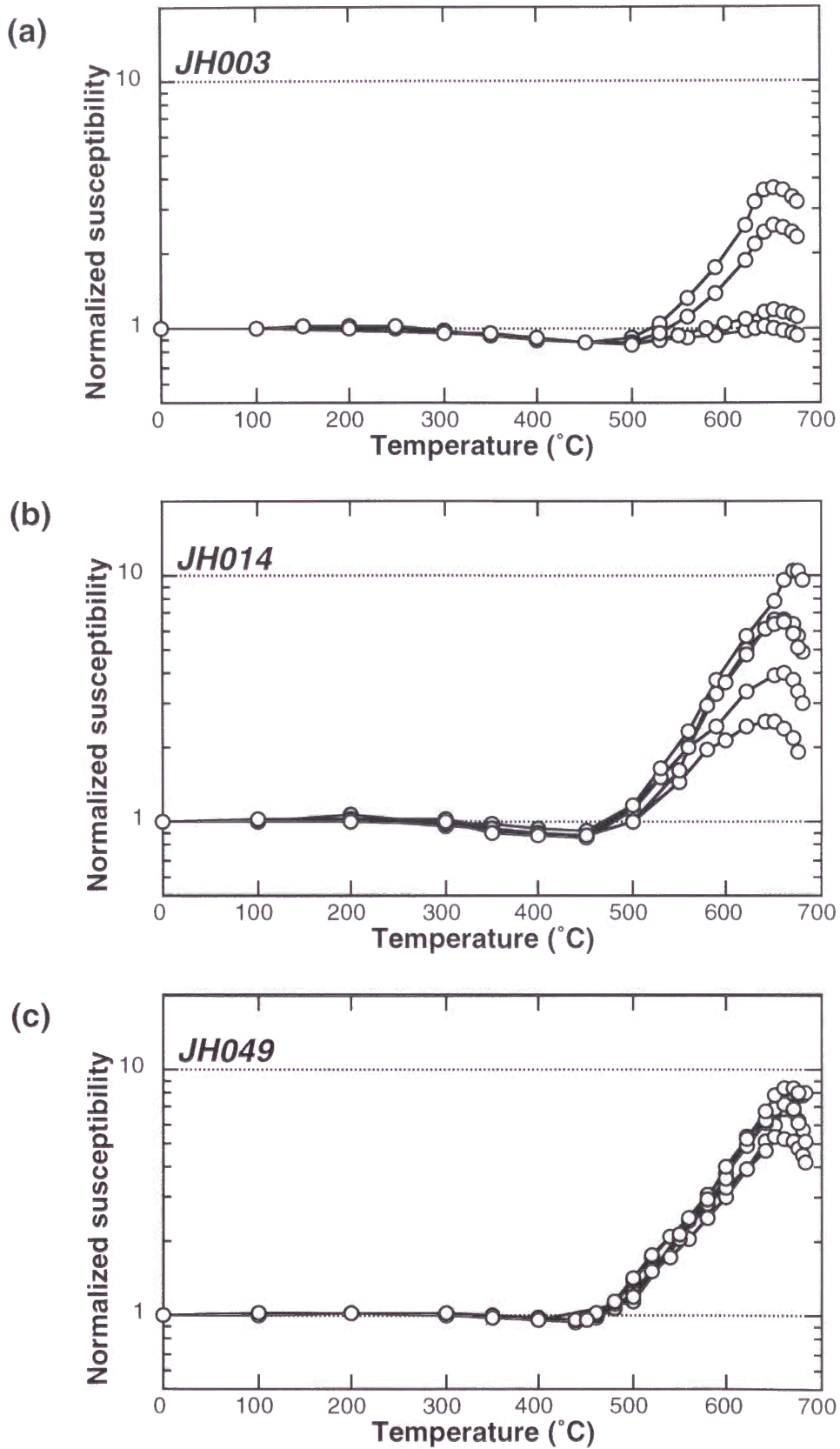
Figure 7. Changes of low-field susceptibility measured at room temperature after each steps of the thermal demagnetization of red bed samples from the Hasandong Formation in Jinju area.
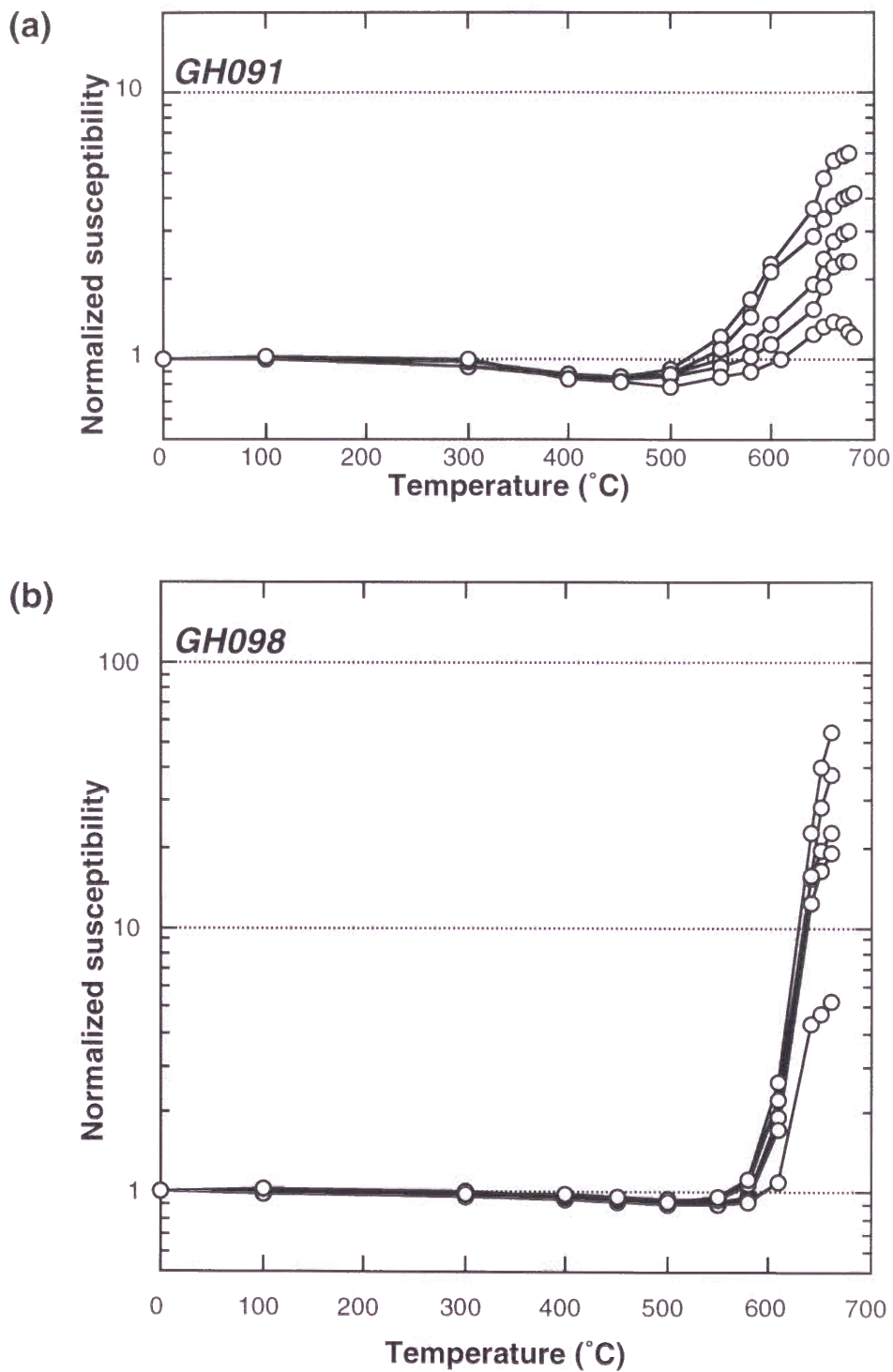
Figure 8. Changes of low-field susceptibility measured at room temperature after each steps of the thermal demagnetization of red bed samples from the Hasandong Formation in Goreong area.

(a) *JH0033*

(b) *JH0151*
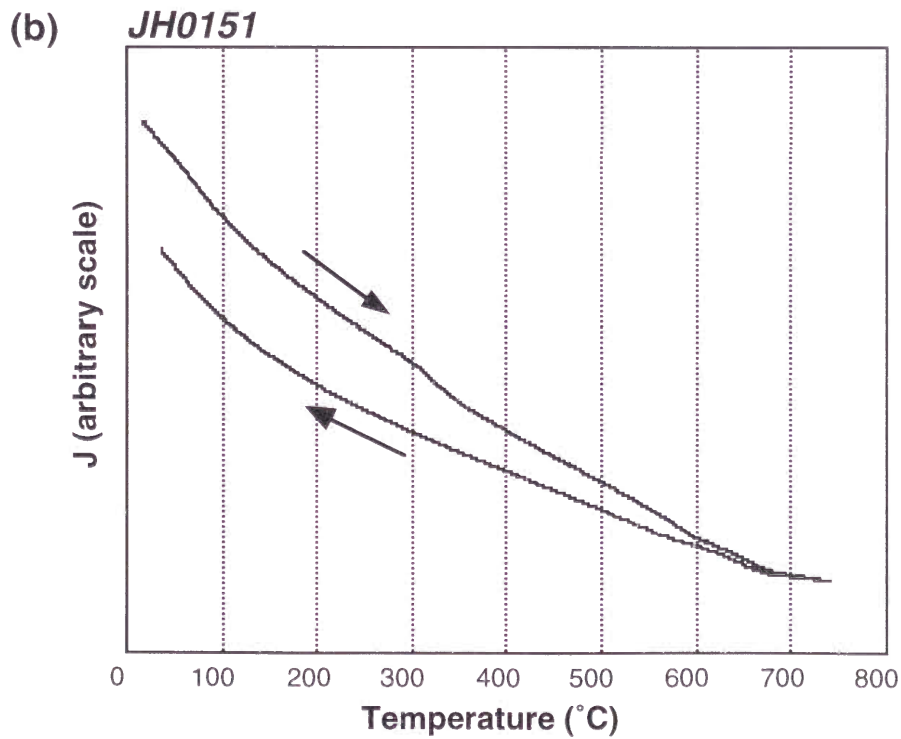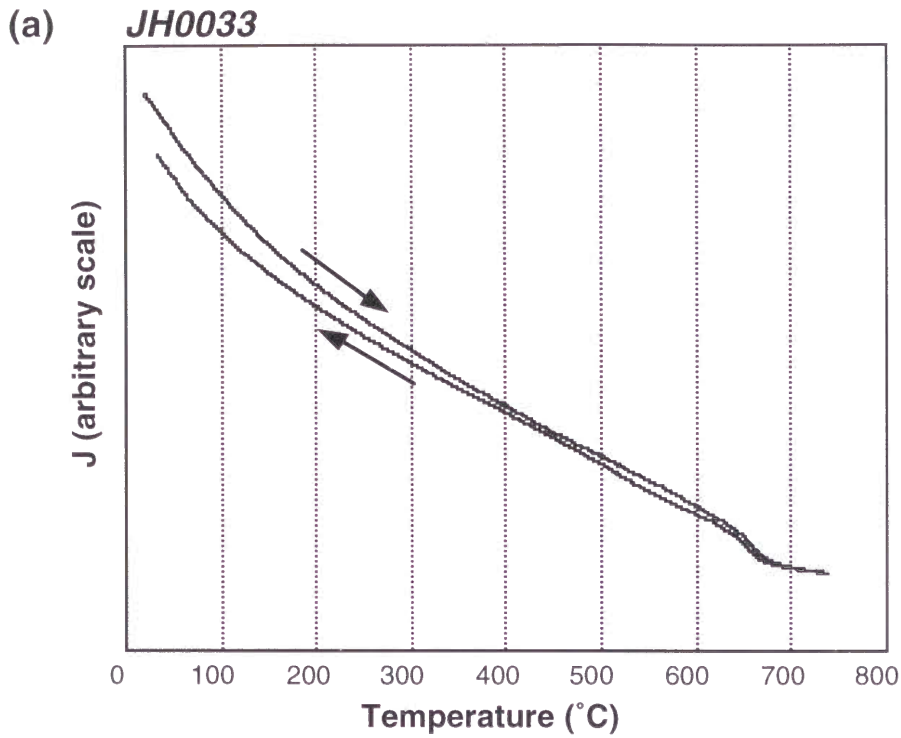
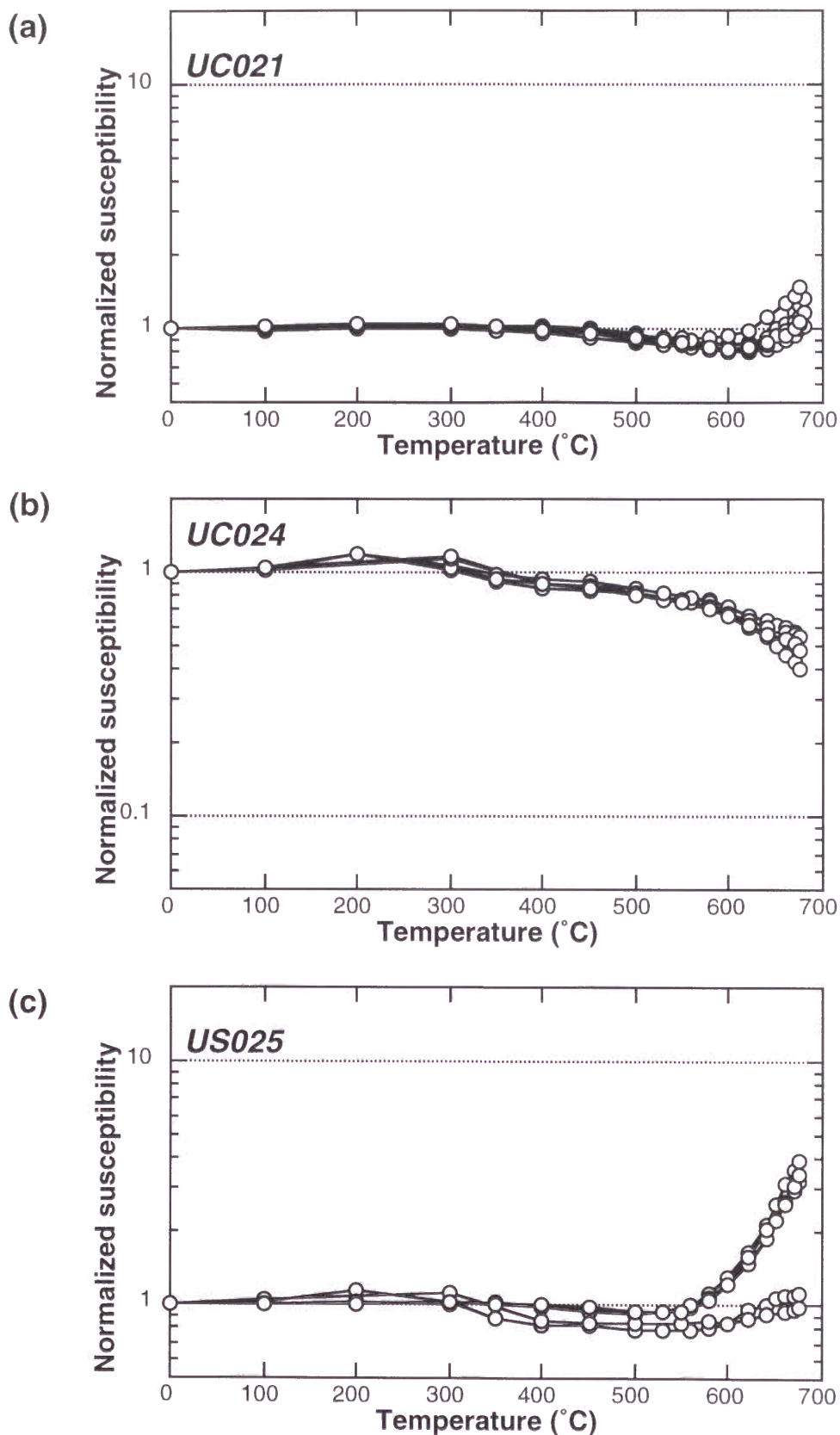**Figure 9.** Thermomagnetic curves for red bed samples from the Hasandong Formation in Jinju area. Strong field magnetization (J) was induced at 0.85 T in air. (a) Only the Curie temperature of hematite (675°C) are shown. (b) Decay of magnetization at ~350°C and ~580°C are identical to the transition of maghemite and the Curie temperature of magnetite. The Curie temperature of hematite are also shown.
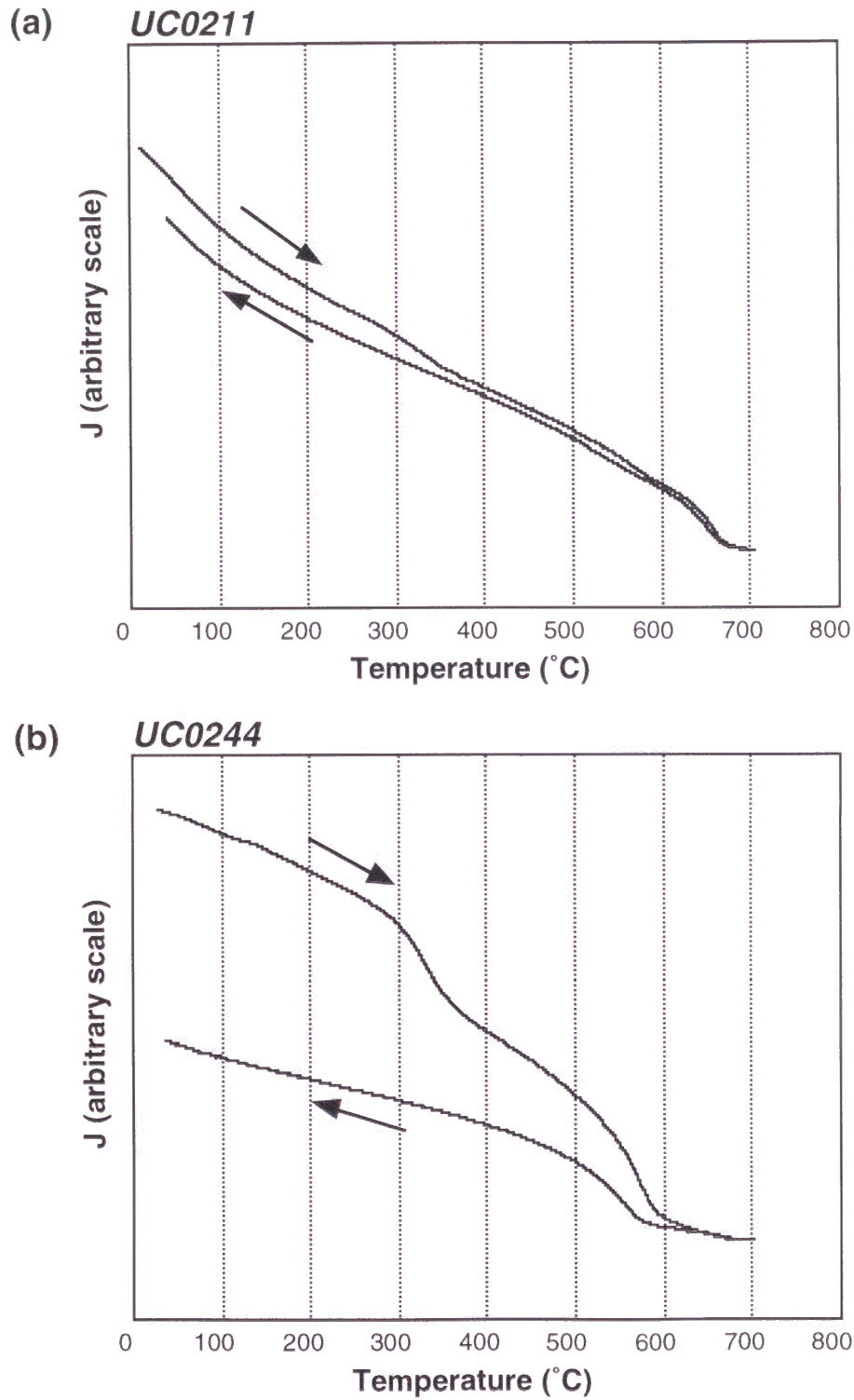
62

(a) *GH0931*

(b) *GH0964*
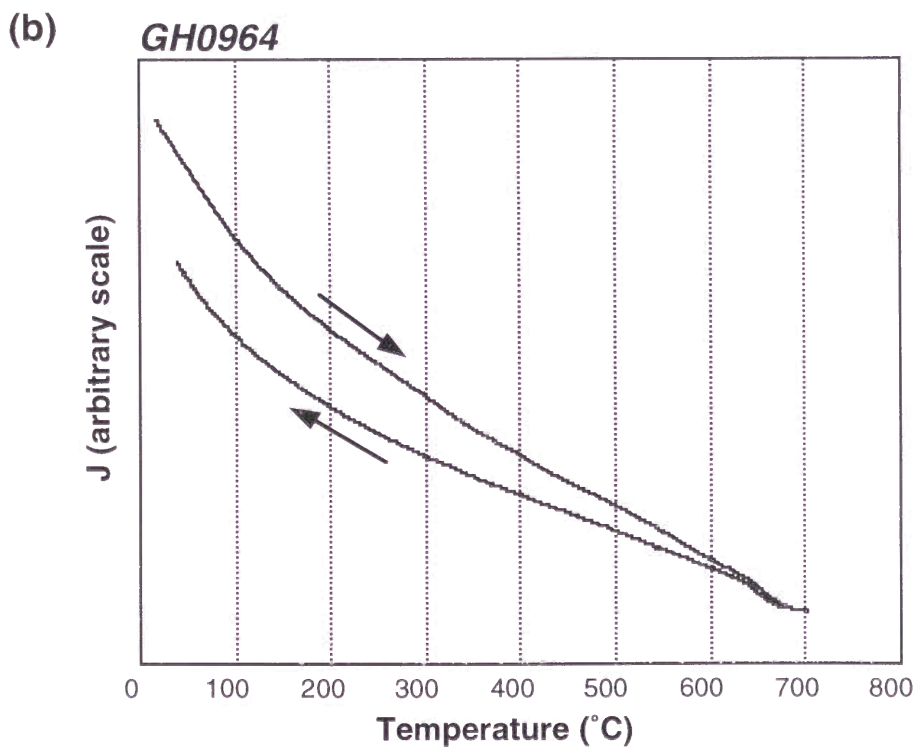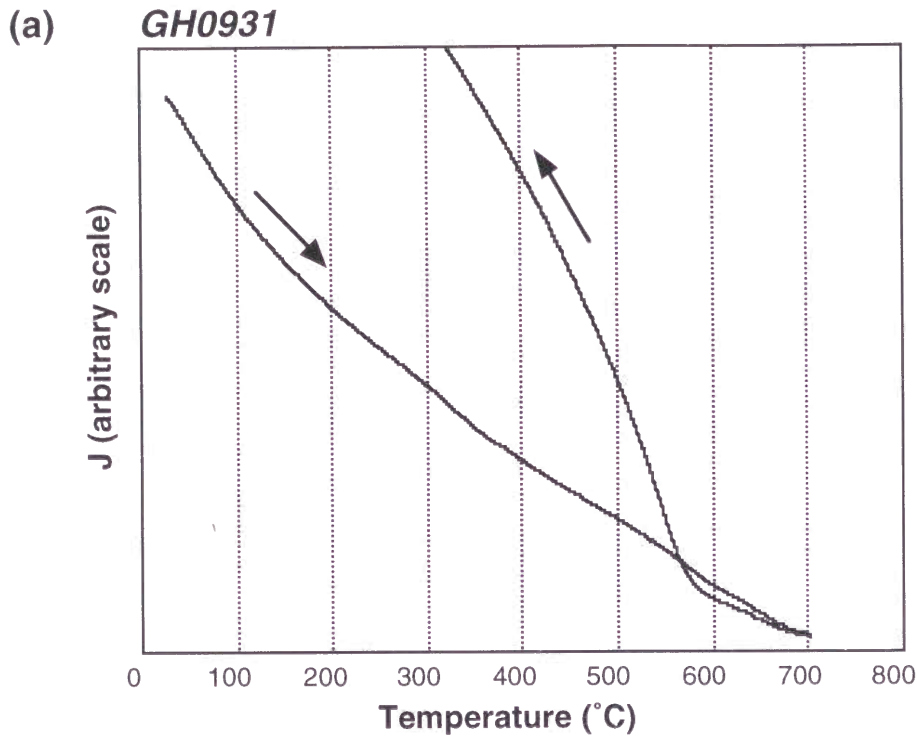
Figure 10. Thermomagnetic curves for red bed samples from the Hasandong Formation in Goreong area. Strong field magnetization (J) was induced at 0.85 T in air. (a) Increase of magnetization around 580°C during the cooling indicates the newly created magnetite due to alterlation. (b) Only the Curie temperature of hematite (675°C) are shown.
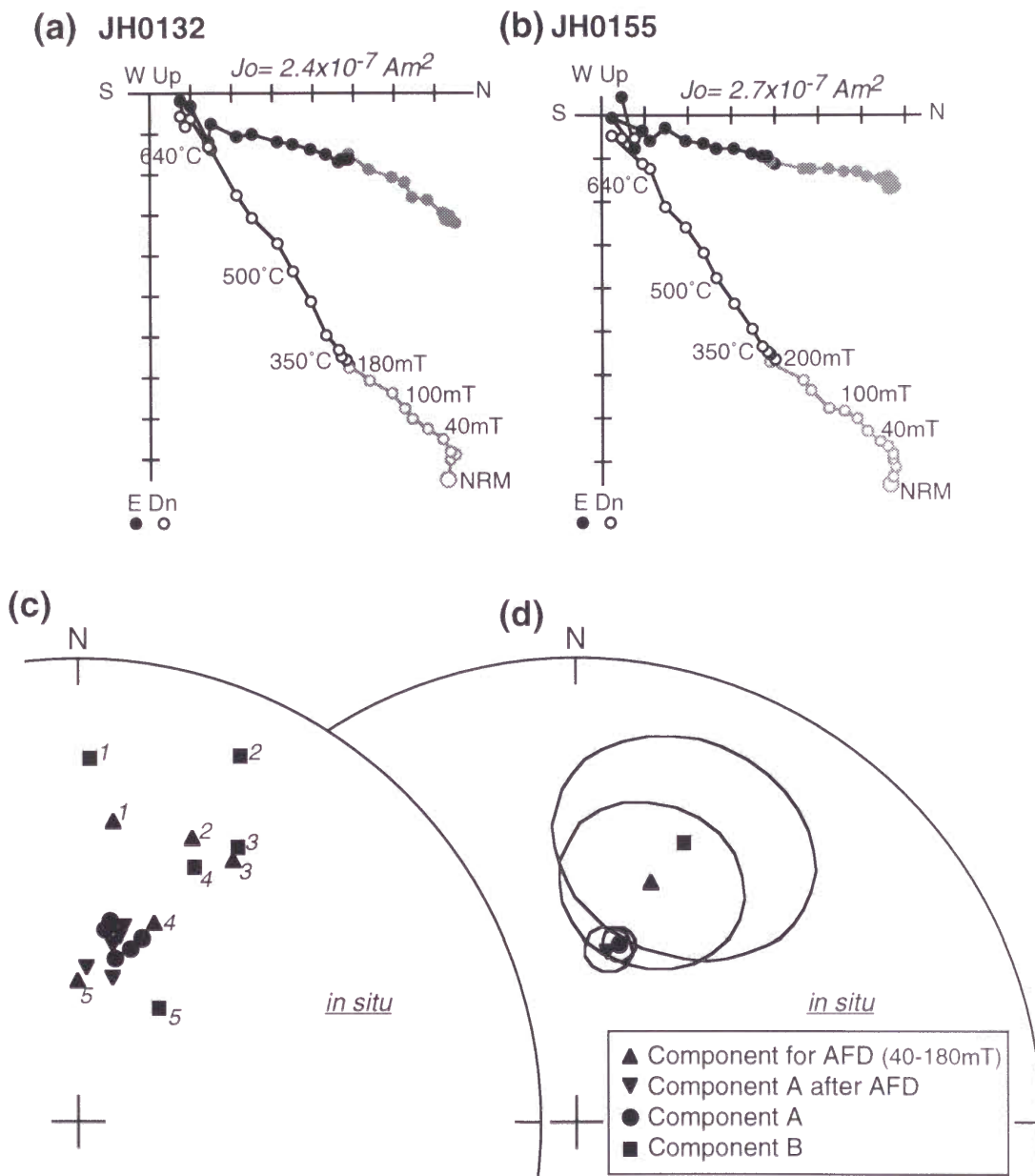
Figure 11. Results of AF demagnetization and successive thermal demagnetization of the red bed samples from the Hasandong Formation in Jinju area. (a)(b) Orthogonal projections of magnetization vector end points during AF (gray) and successive thermal demagnetizations (black) are shown for representative samples in geographic coordinate. (c) Sample directions of each component determined by AF and thermal demagnetization are plotted on equal area projection. Associated numbers mean the same sample. (d) Mean directions of each component for five samples shown in (c) are plotted with 95% confidence limit on equal area projection .

64
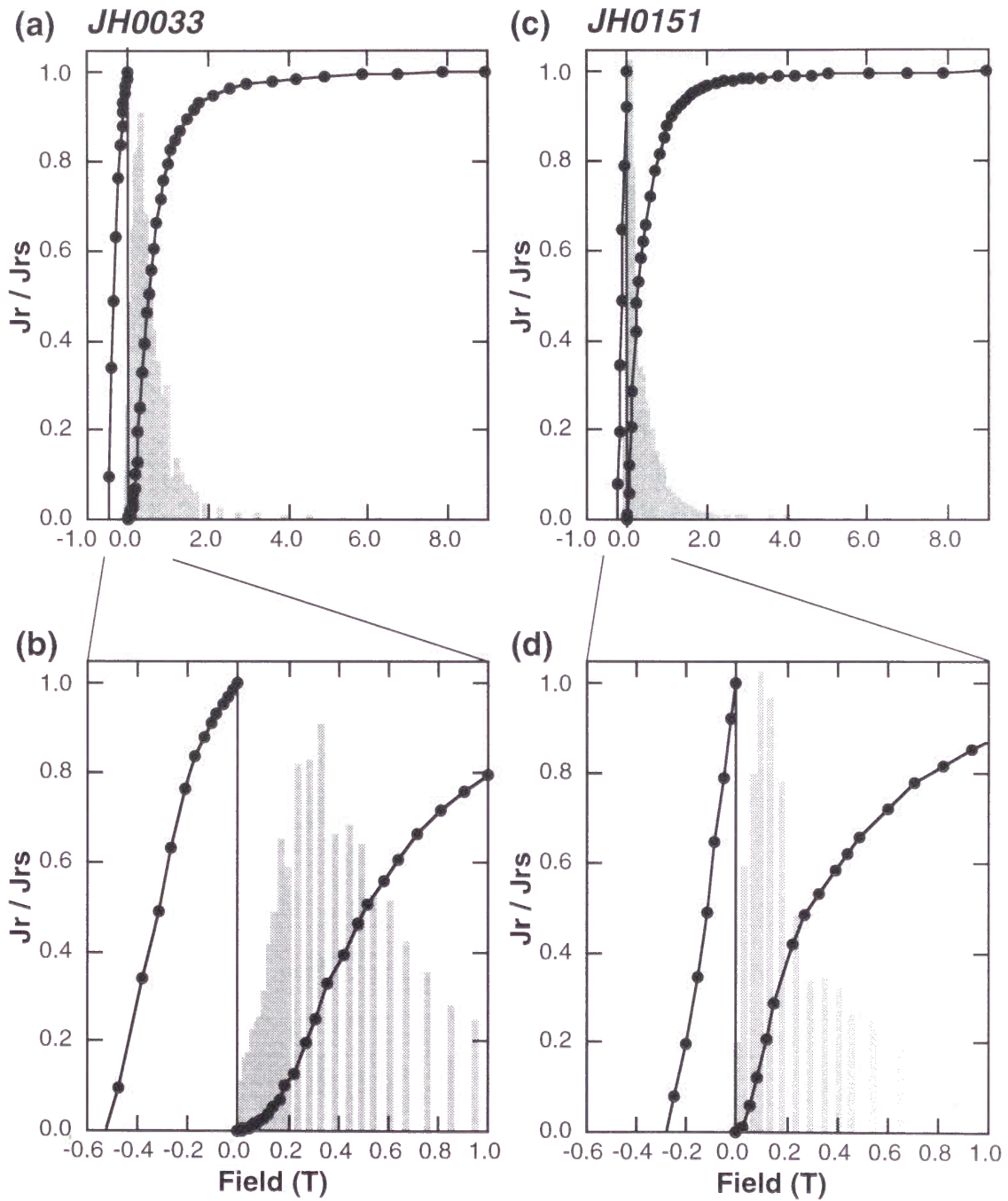
Figure 12. IRM acquisition curve and back-field demagnetization for red bed samples from the Hasandong Formation in Jinju area. Magnetic coercivity spectrum are shown as gray bars in arbitrary scale. The low coercivity part for (a) and (c) are enlarged to (b) and (d), respectively.

(a) *JH0033*

(b) *JH0151*

(c) *JH0184*
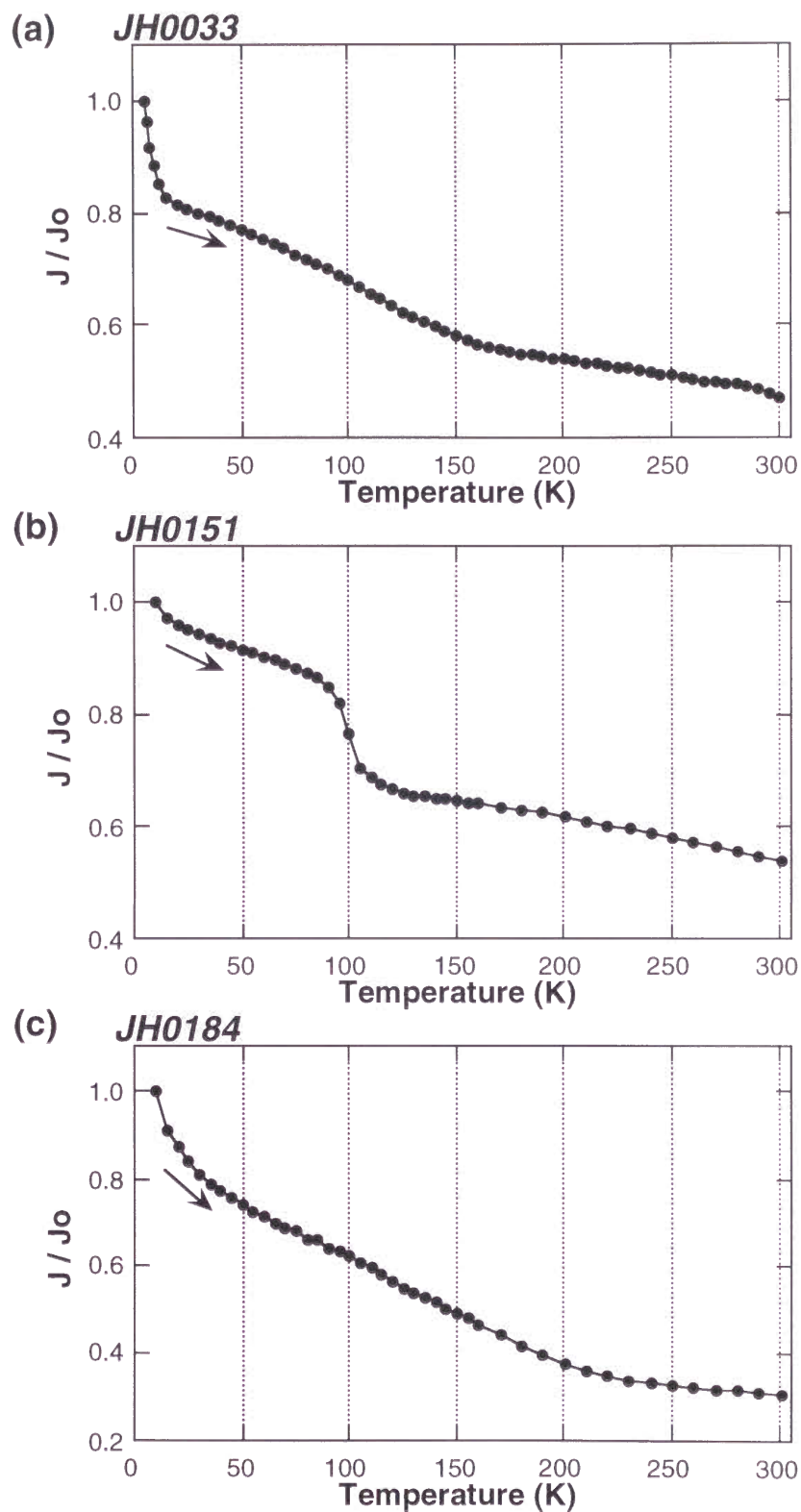
Figure 13. Low temperature measurements of red bed samples from the Hasandong Formation in Jinju area. (a), (b) and (c) are the results of warming mode. The Verwey transition of magnetite (maghenite) are shown at ~100 K only in (b). (d), (e) and (f) are the results of cooling-warming mode. Gradually decrease of IRM during cooling and recovery during warming are shown at wide range of temperature of 150~250 K. The verwey transition around 120 K is also shown in (e) and (f).

(d) *JH0033*

(e) *JH0151*

(9.25T)

(f) *JH0184*
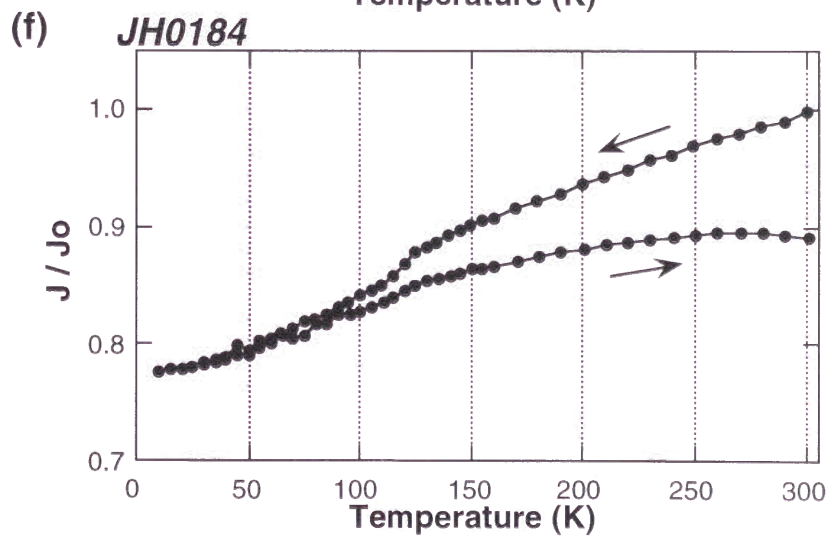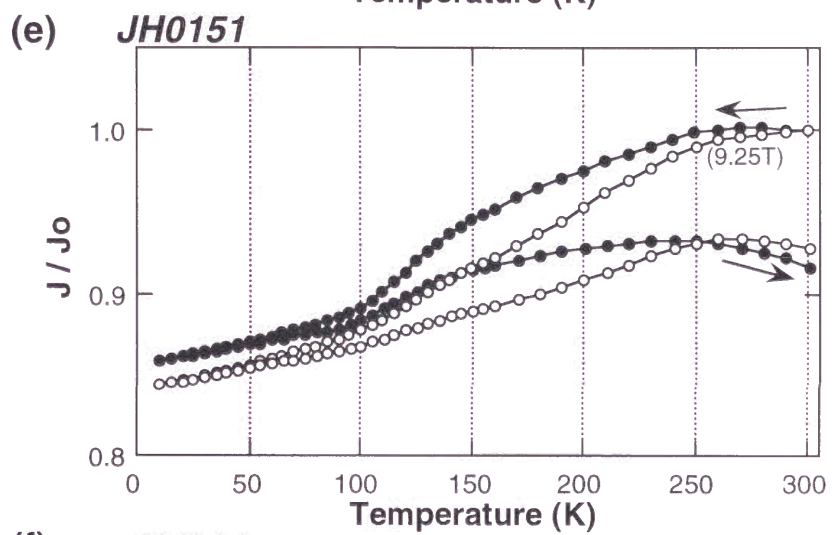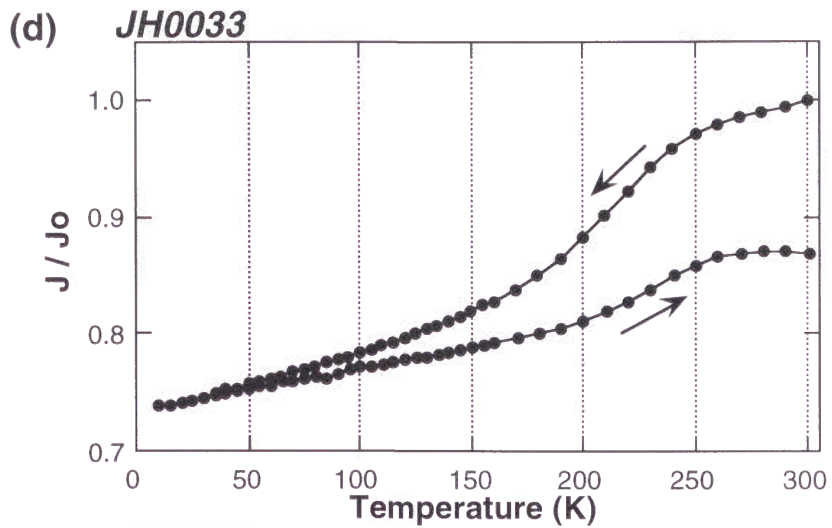
Figure 13. (continued)

67
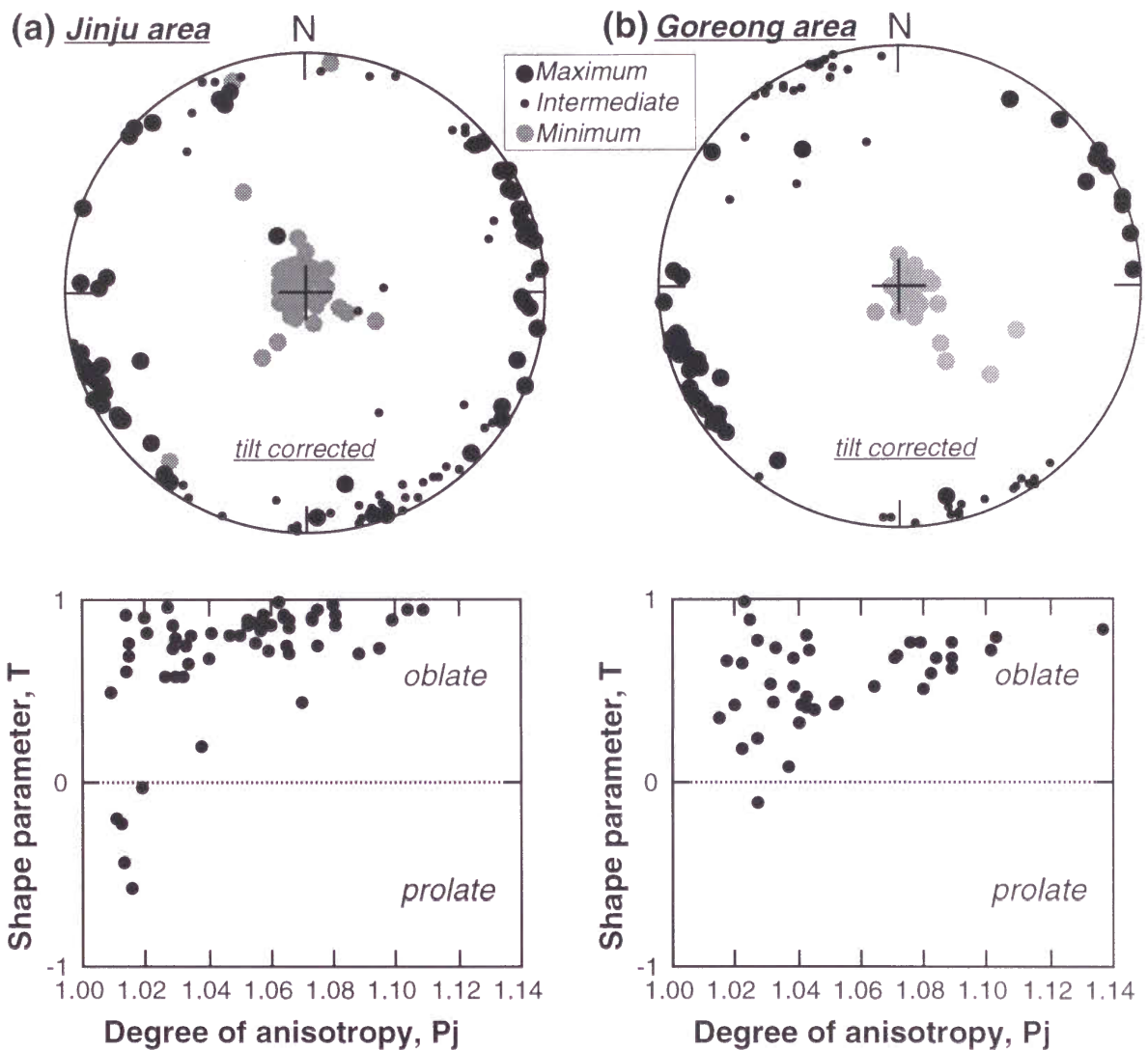
Figure 14. Anisotropy of magnetic susceptibility of red bed samples from the Hasandong Formation in Jinju area (a) and in Goreong area (b). (Top) AMS directions on equal area projection in stratigraphic coordinate. (Bottom) Hrouda-Jelinek anisotropy diagram for AMS degree (Pj) and the shape parameter (T).

68
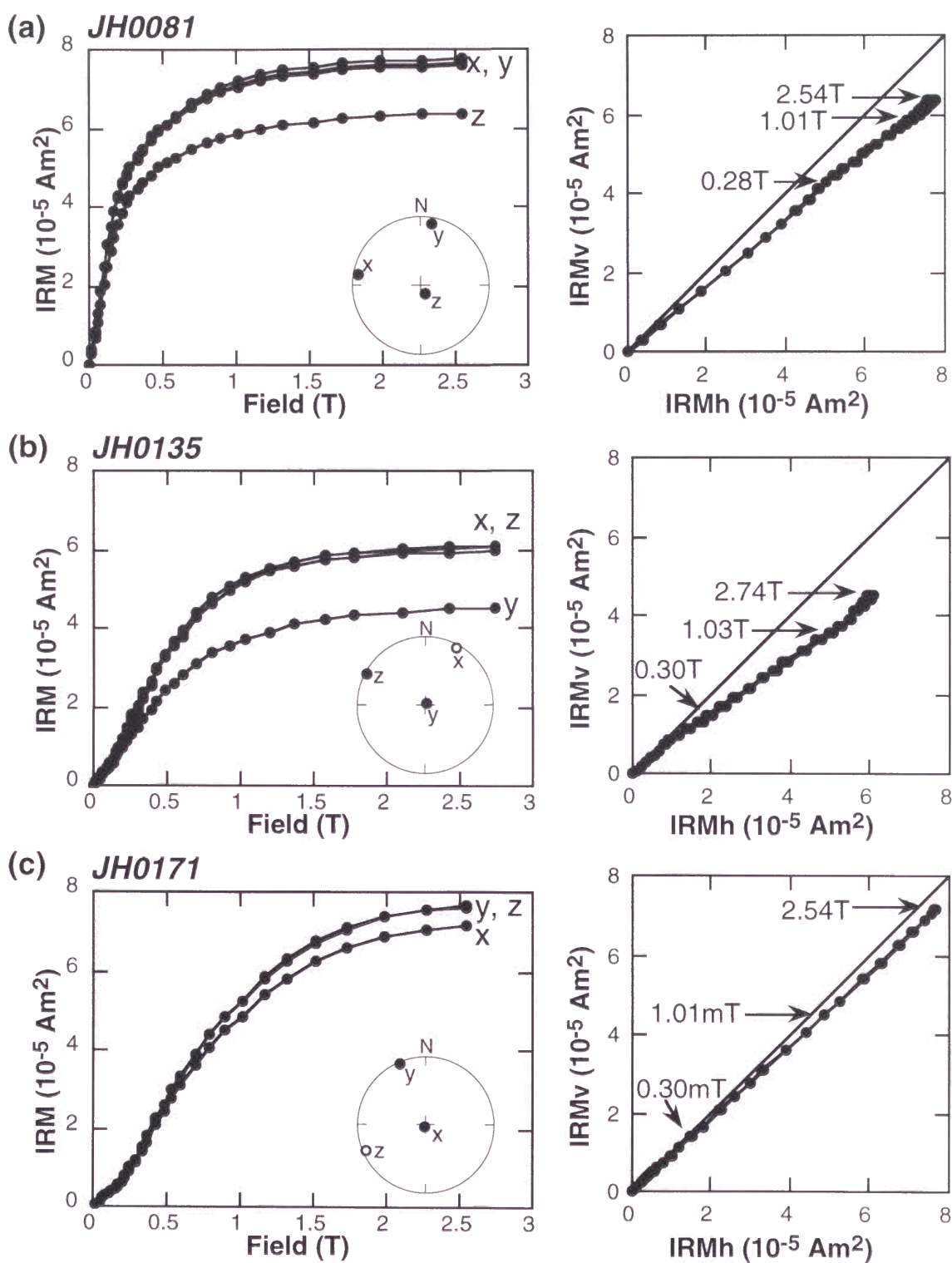
Figure 15. (Left) IRM acquisition curves to three orthogonal axes. Each direction on equal area projection are inseted. (Right) Plots of the IRMv to IRMh at the same applied field level.

(a) UC0214
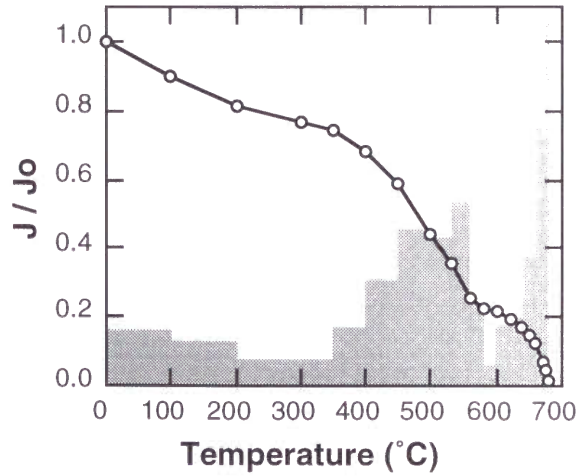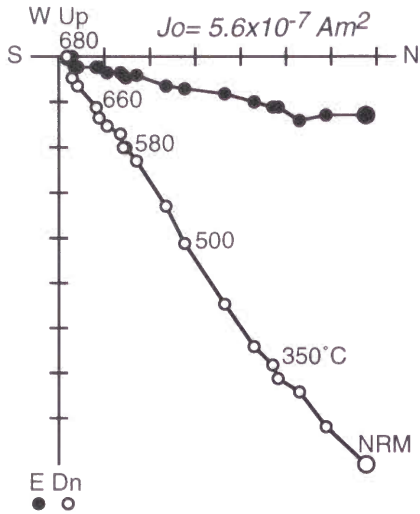
(b) UC0244
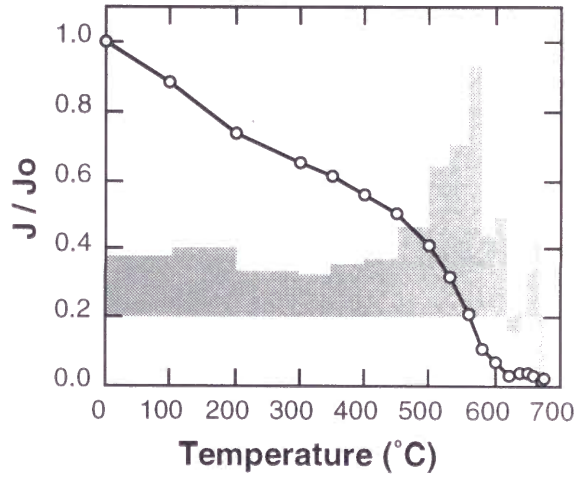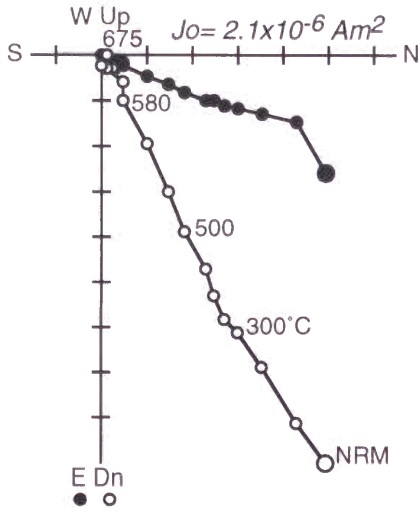
(c) US0253
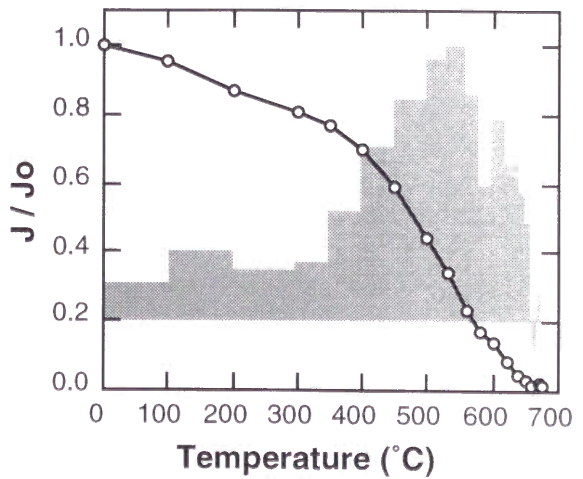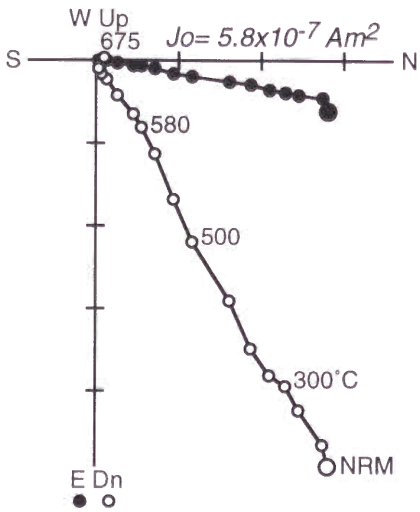
Figure 16. Results of representative samples of red beds from the Chilgok and the Shilla Formations in Jinju area during thermal demagnetization. Details are same as Fig. 5.

70

(a)

(b)

(c)

Figure 17. Changes of low-field susceptibility measured at room temperature after each steps of the thermal demagnetization of red bed samples from the Chilgok and the Shilla Formations in Jinju area.

(a) *UC0211*

(b) *UC0244*

Figure 18. Thermomagnetic curves for red bed samples from the Chilgok Formation in Jinju area. Strong field magnetization (J) was induced at 0.85 T in air. (a) The Curie temperature of hematite (675°C) are shown. (b) Large decay of magnetization at ~350°C and ~580°C are identical to the transition of maghemite and the Curie temperature of magnetite.
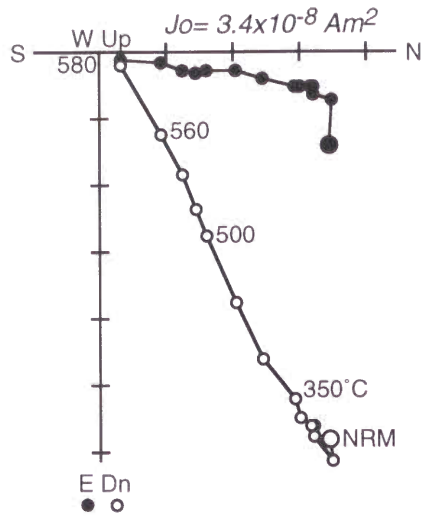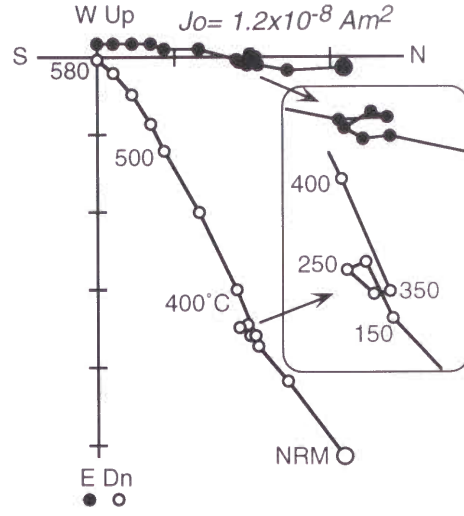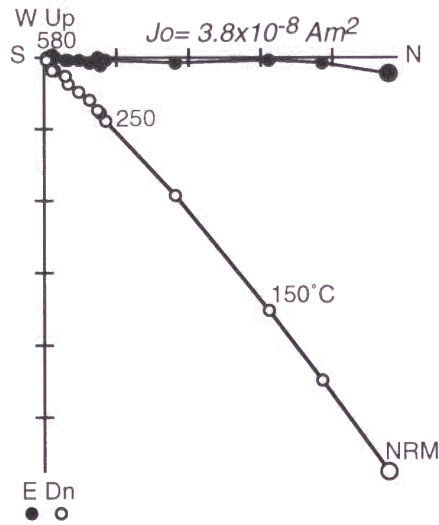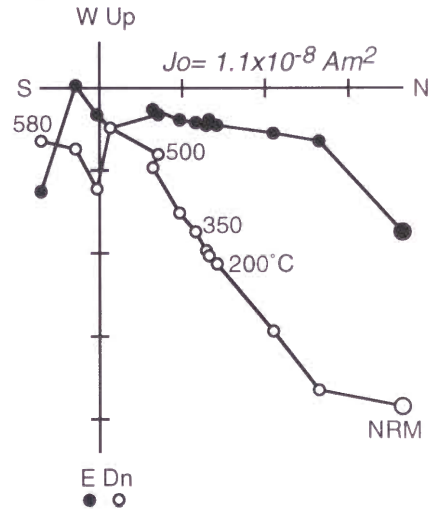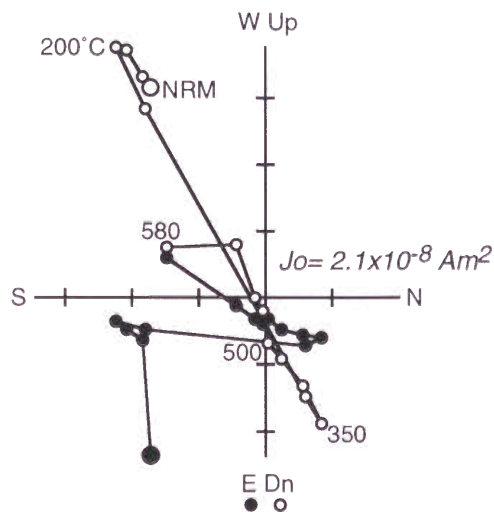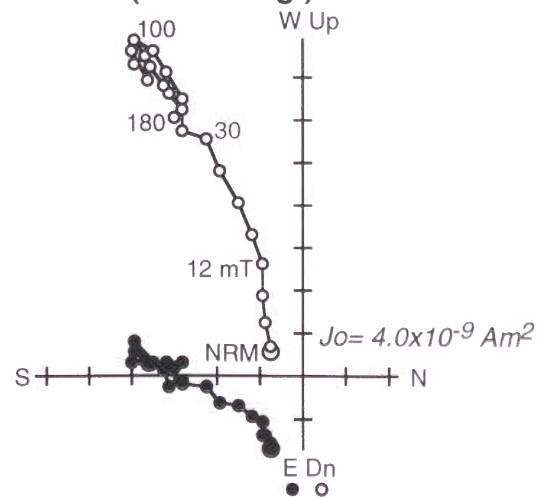
Figure 19. Results of representative samples of non-red sedimentary rocks from the Jinju Formation in Jinju area during thermal demagnetization (a)~(e) and AF demagnetization (f). Orthogonal projections of magnetization vector end points are shown in geographic coordinate.

73

(a) *JJ0393*

(b) *JJ0393 (in air)*

(c) *JJ0393 (in Ar gas)*
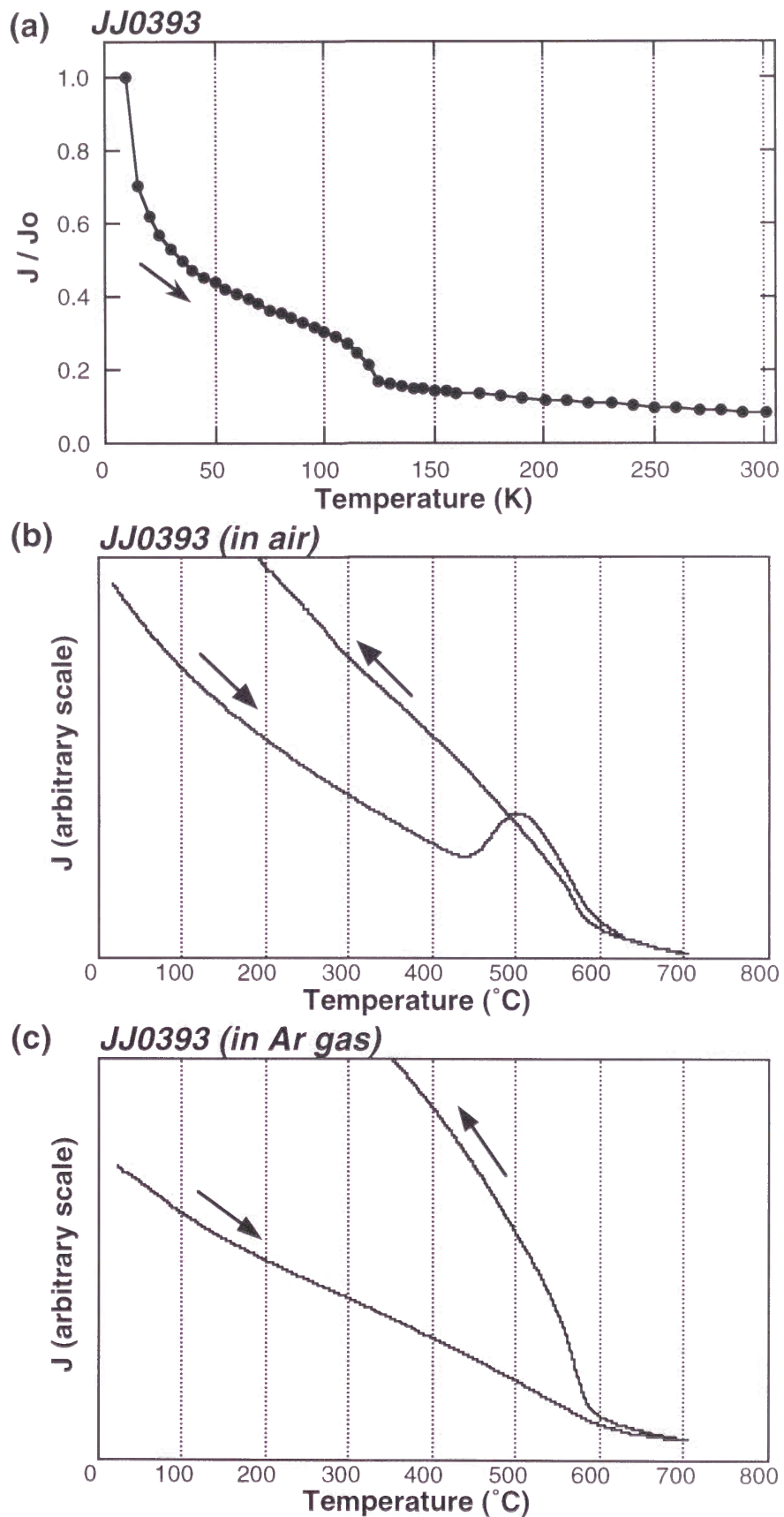
Figure 20. Rock magnetic properties of sample of non-red sediments from the Jinju Formation, which revealed the reversed polarity component. Low-temperature measurement in warming mode (a) and thermomagnetic curves in air (a) and in Ar gas (b) are shown.

74

(a)

N

in situ

N

tilt corrected
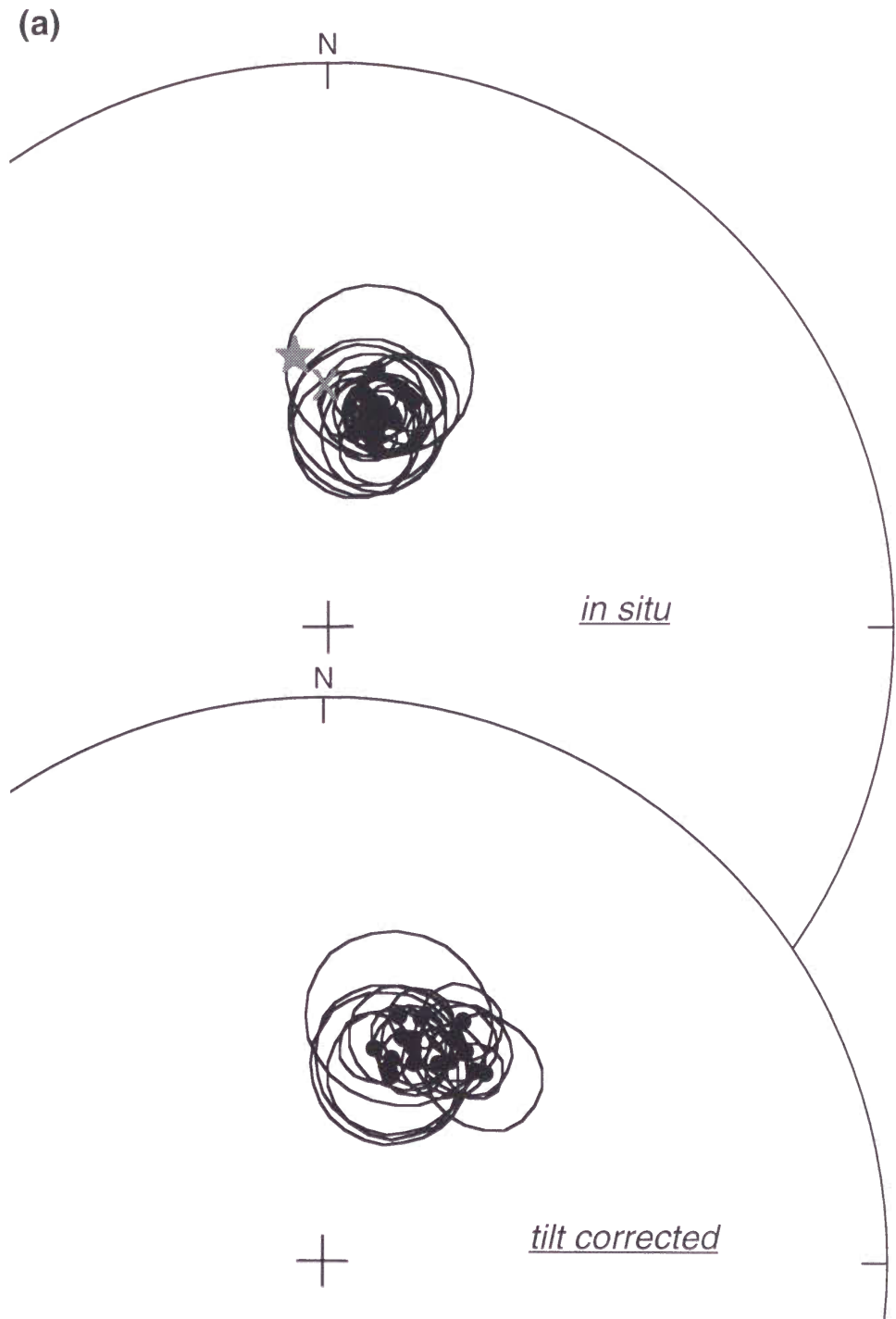
Figure 21. Site mean directions of component A of red beds with 95% confidence limits on equal area projection, from the Hasandong Formation in Jinju area (a), from the Hasandong Formation in Goreong area (b) and from the Chilgok and the Shilla Formations in Jinju area (c). Top is for in situ directions. Star and cross denote the present geomagnetic field direction and the geocentric axial dipole field direction, respectively. Bottom is for tilt-corrected directions.

(b)

in situ

tilt corrected

Figure 21. (continued)

76

(c)

N

in situ

N

tilt corrected
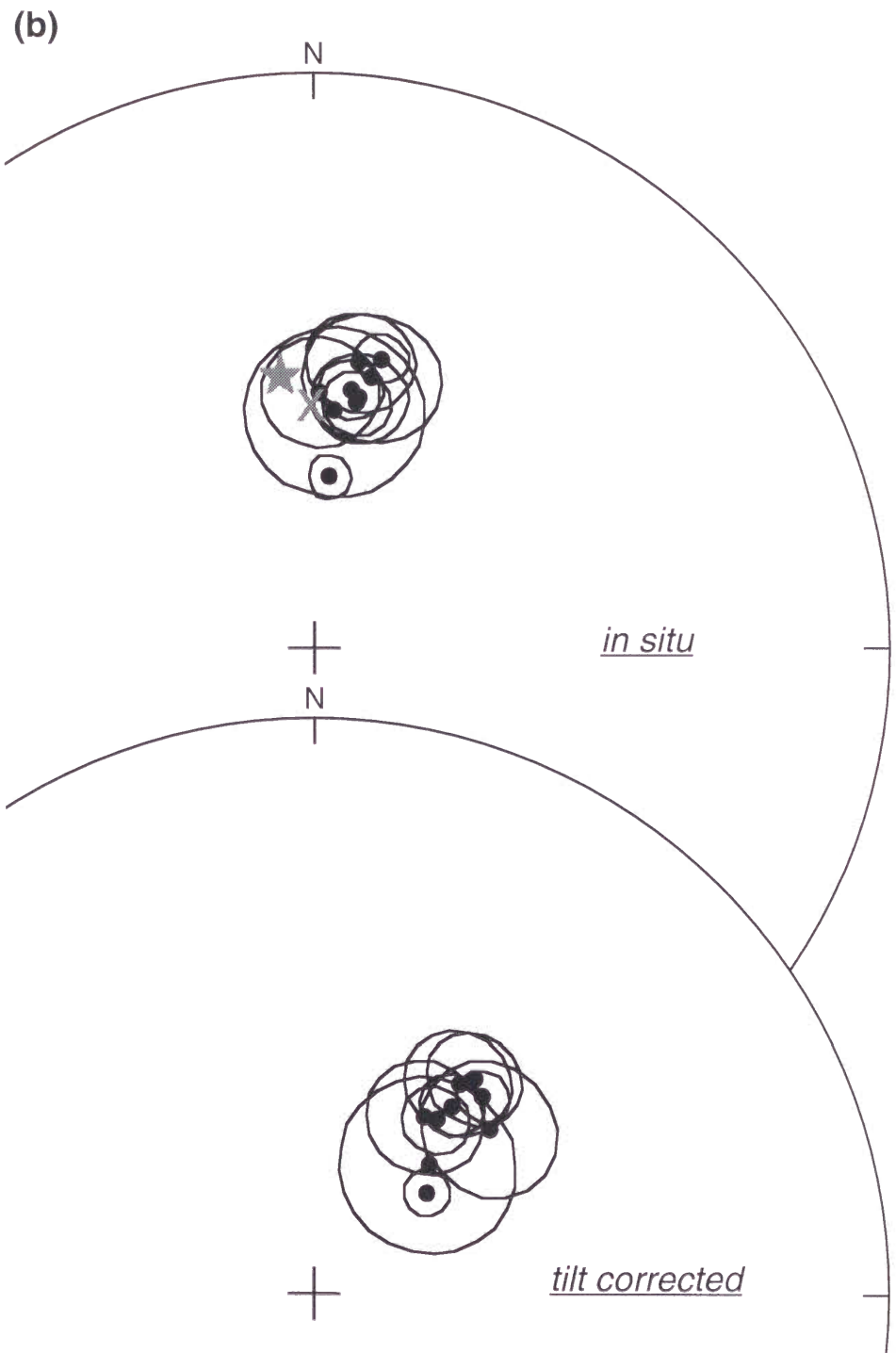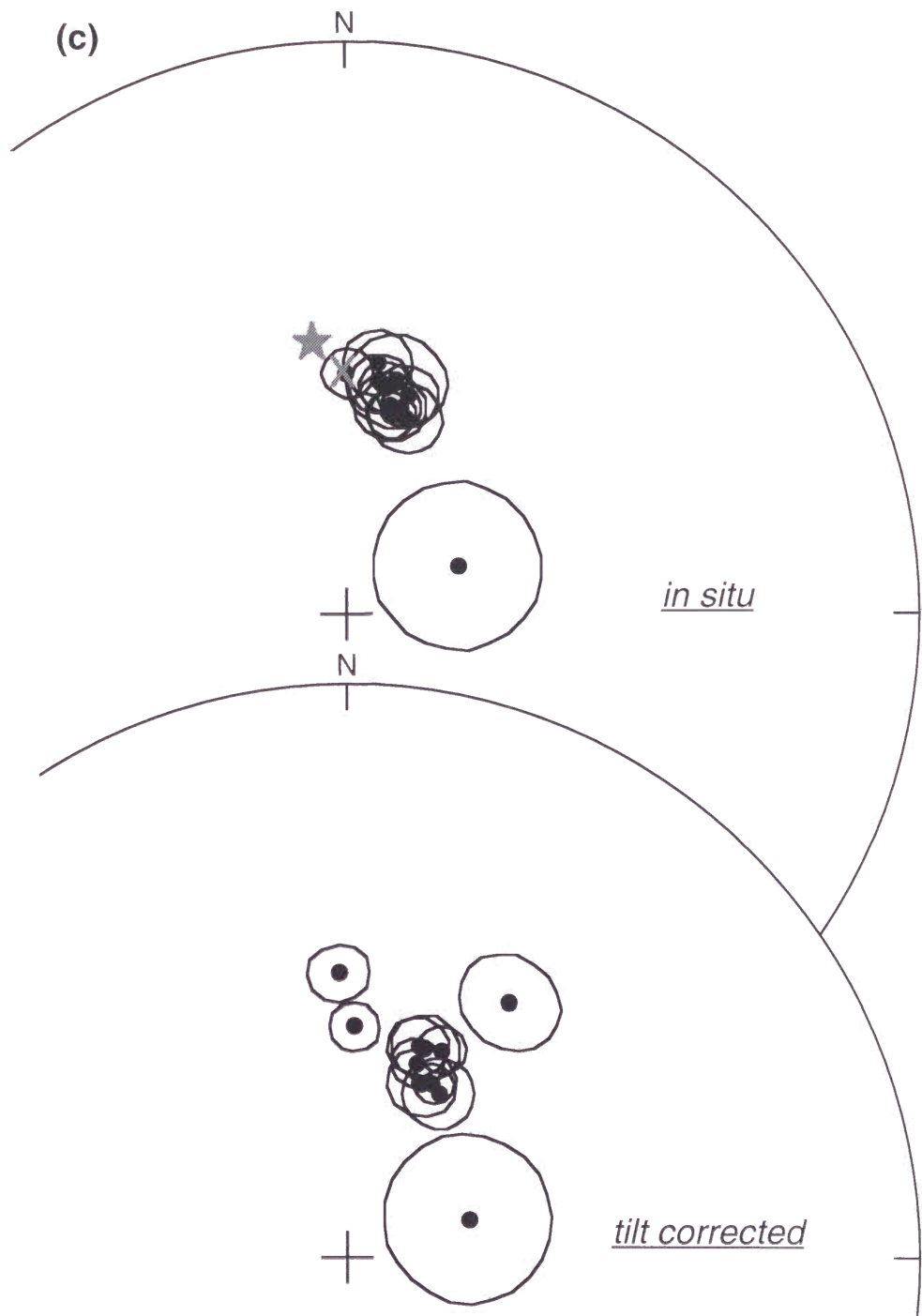
Figure 21. (continued)
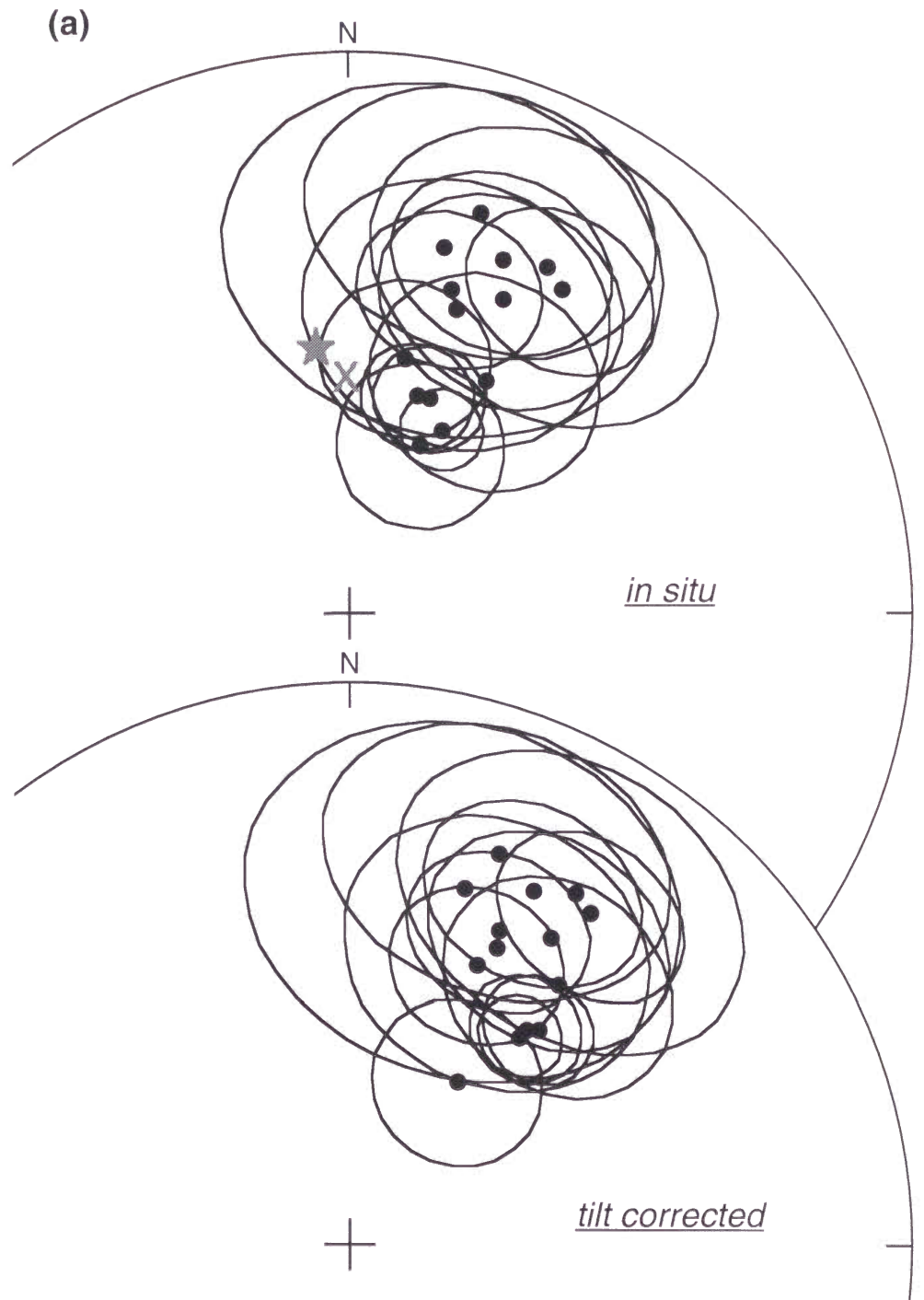
Figure 22. Site mean directions of component B of red beds with 95% confidence limits on equal area projection, from the Hasandong Formation in Jinju area (a) and from the Chilgok and the Shilla Formations in Jinju area (b). Details are same as Fig. 21.
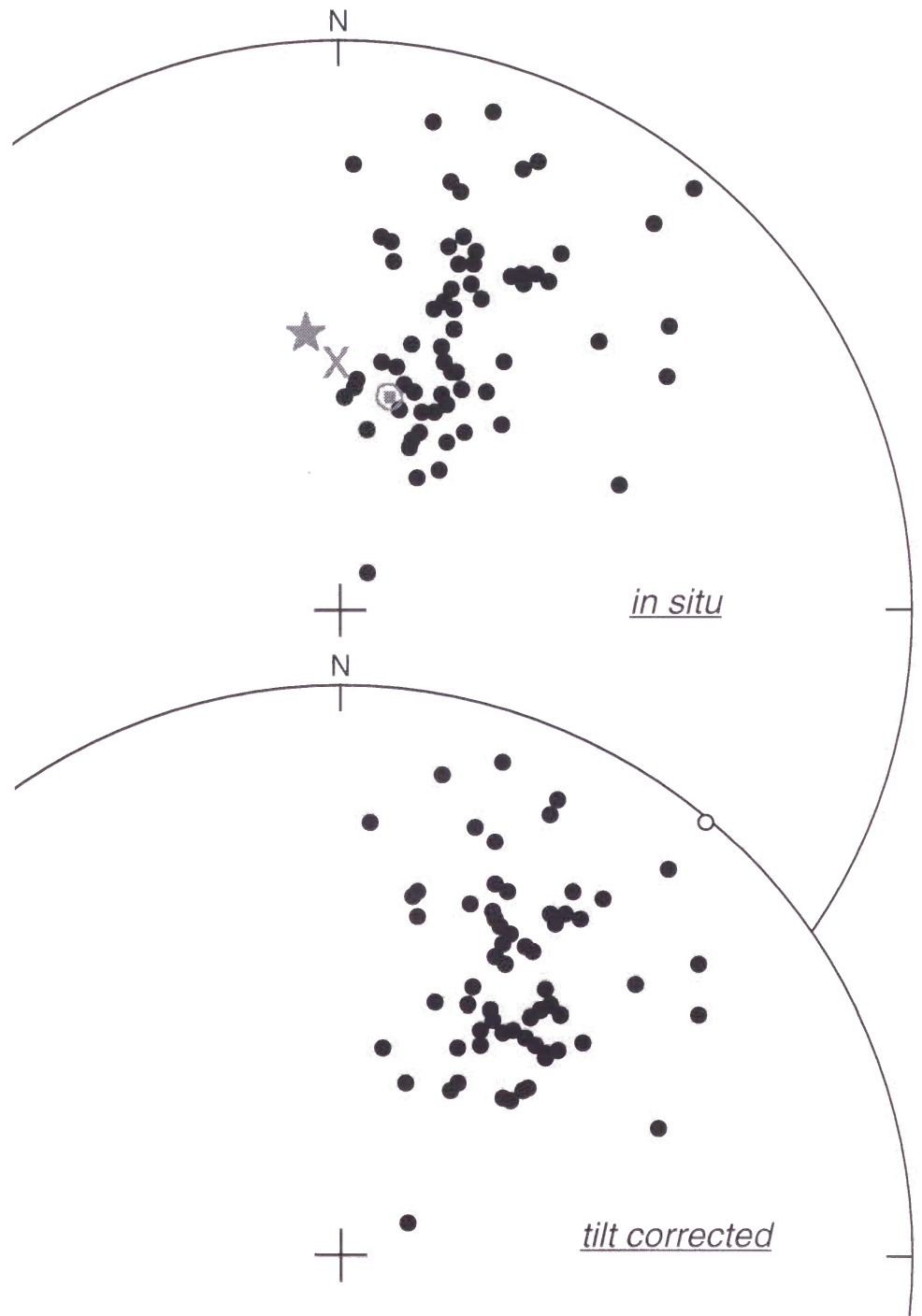
78

(b)

N

in situ

N

tilt corrected
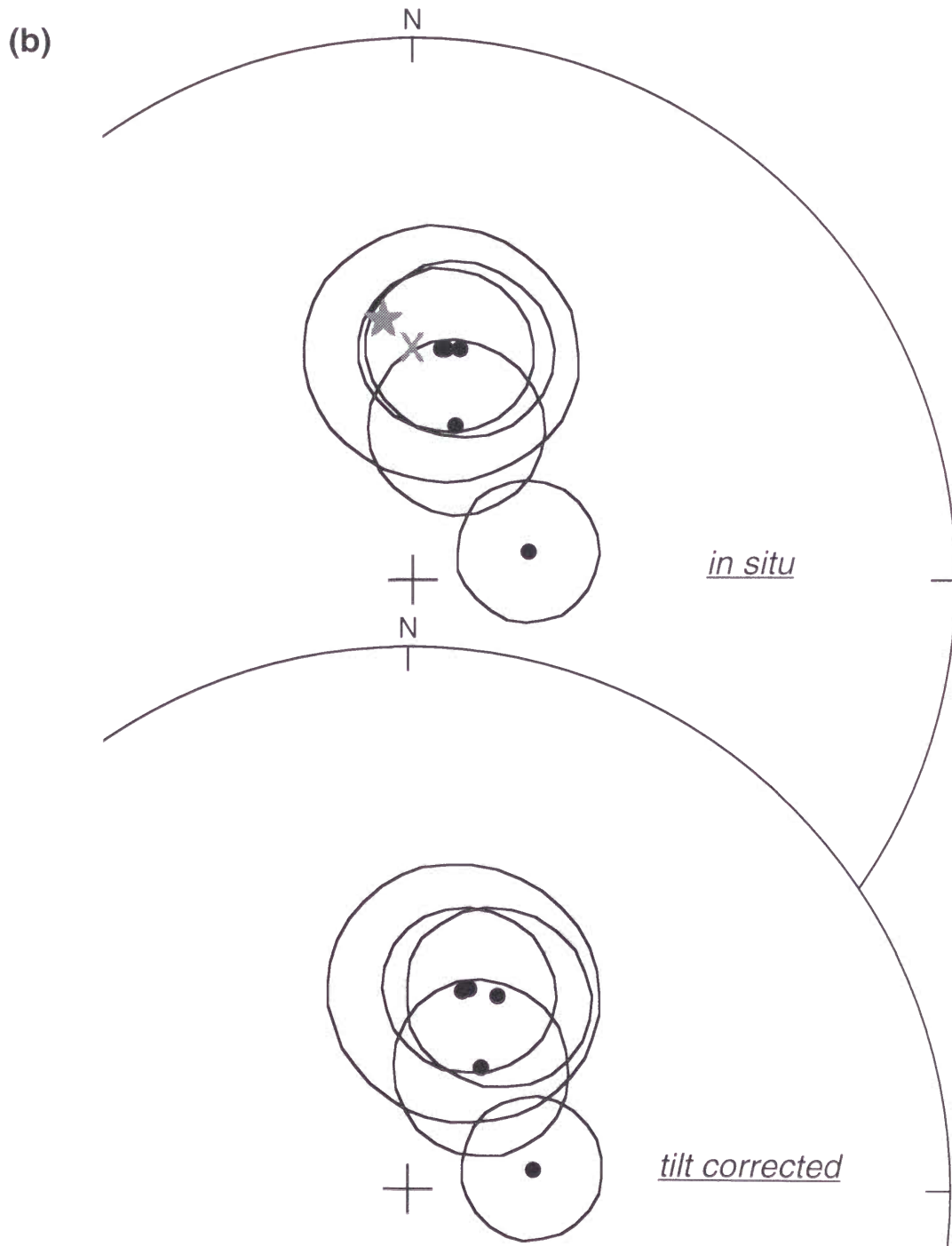
Figure 22. (continued)

Figure 23. Dispersion of directions of component B from the Hasandong Formation in Jinju area. Gray square indicate the mean directions of formation-mean of component A and magnetite component with 95% confidence limit. Details are same as Fig. 21.
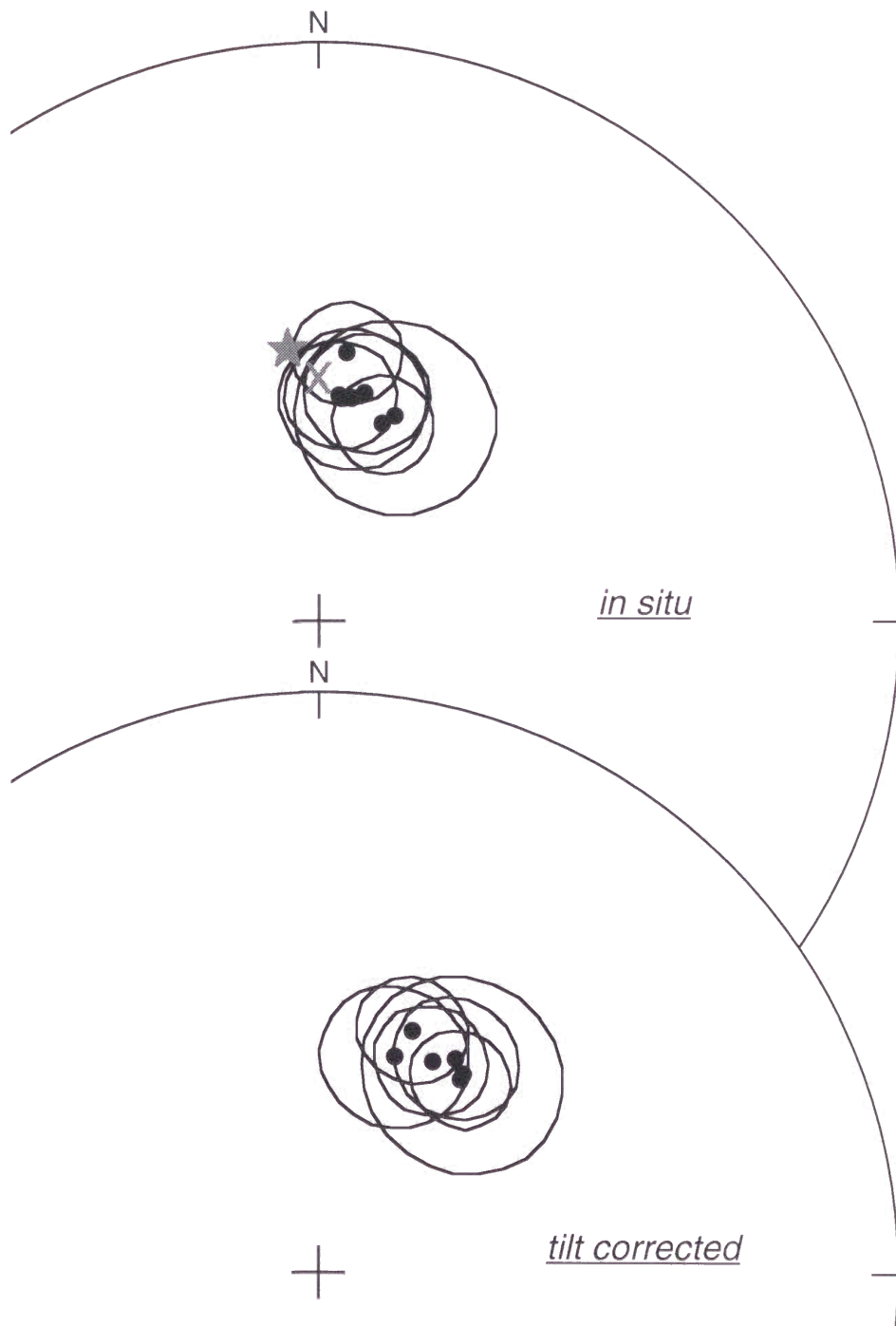
Figure 24. Site mean directions from non-red sedimentary rocks of the Jinju Formation with 95% confidence limits on equal area projection. Details are same as Fig. 21.
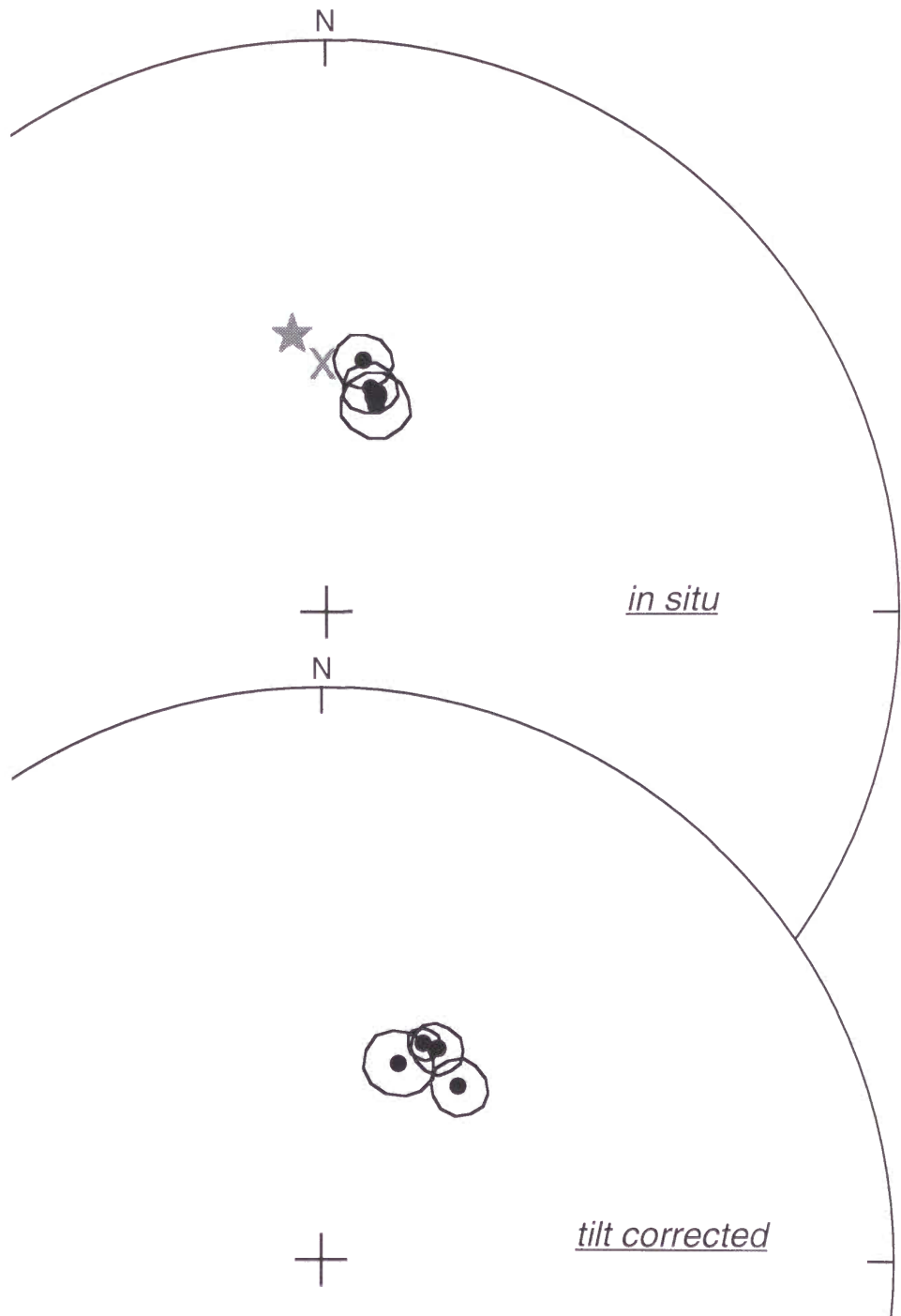
Figure 25. Formation mean directions of component A from red beds and of magnetite component from non-red sedimentary rocks with 95% confidence limits on equal area projection. Details are same as Fig. 21.
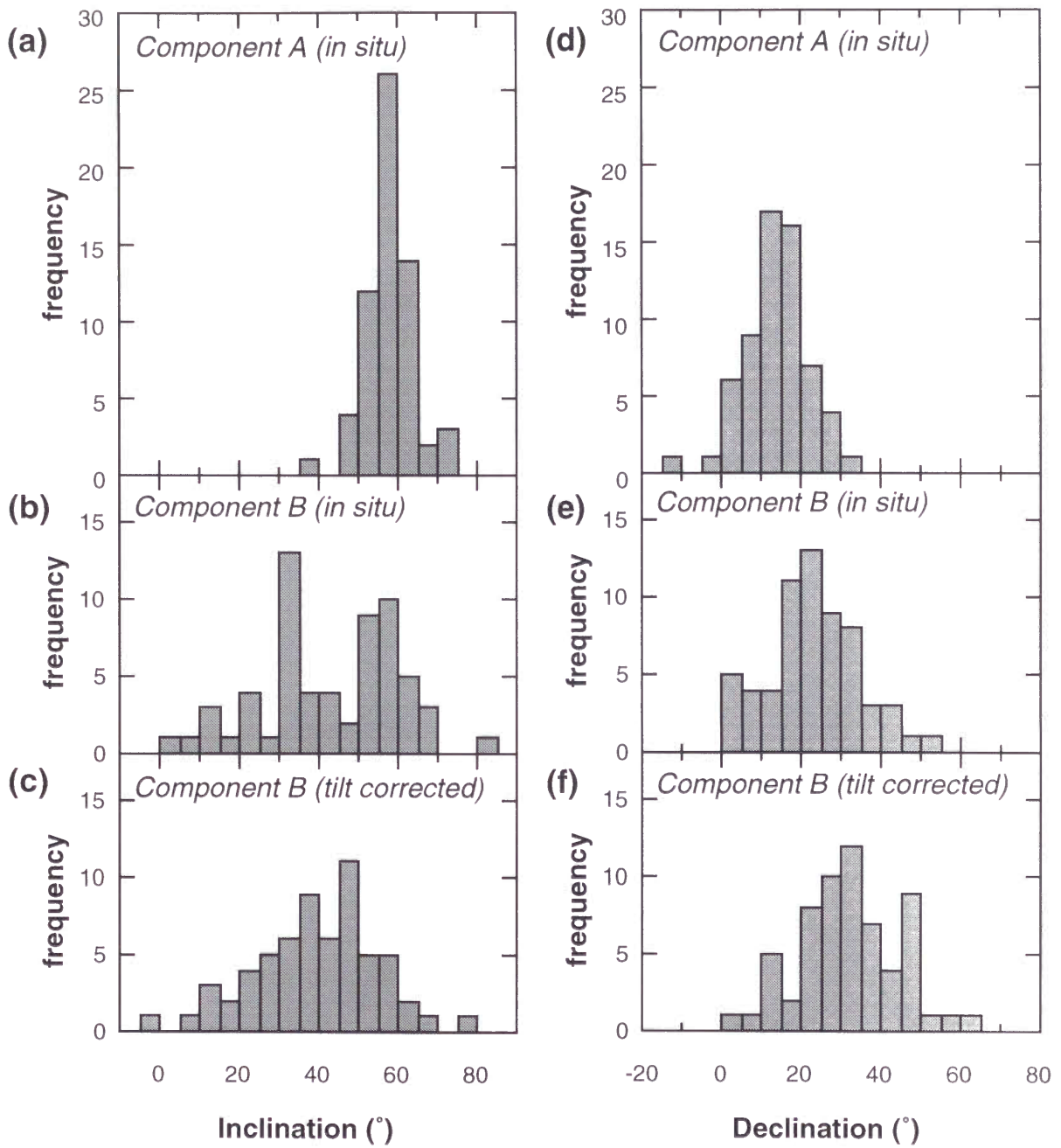
Figure 26. Histograms of inclinations (a,b,c) and declinations (d,e,f) of the directions for samples of the Hasandong Formation. (a) and (d) for component A before tilt-correction, (b) and (e) for component B before tilt-correction and (c) and (f) for component B after tilt-correction.
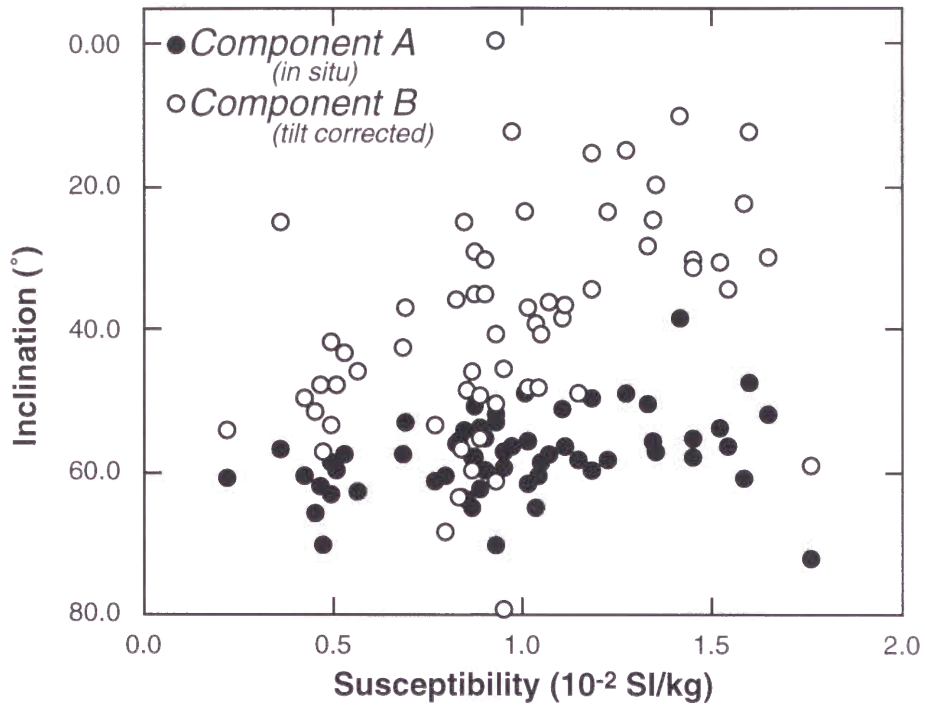
83

Figure 27. Inclination value to low-field susceptibility. Inclination of component B has shallower when susceptibility is larger, while that of component A does not depend on susceptibility.
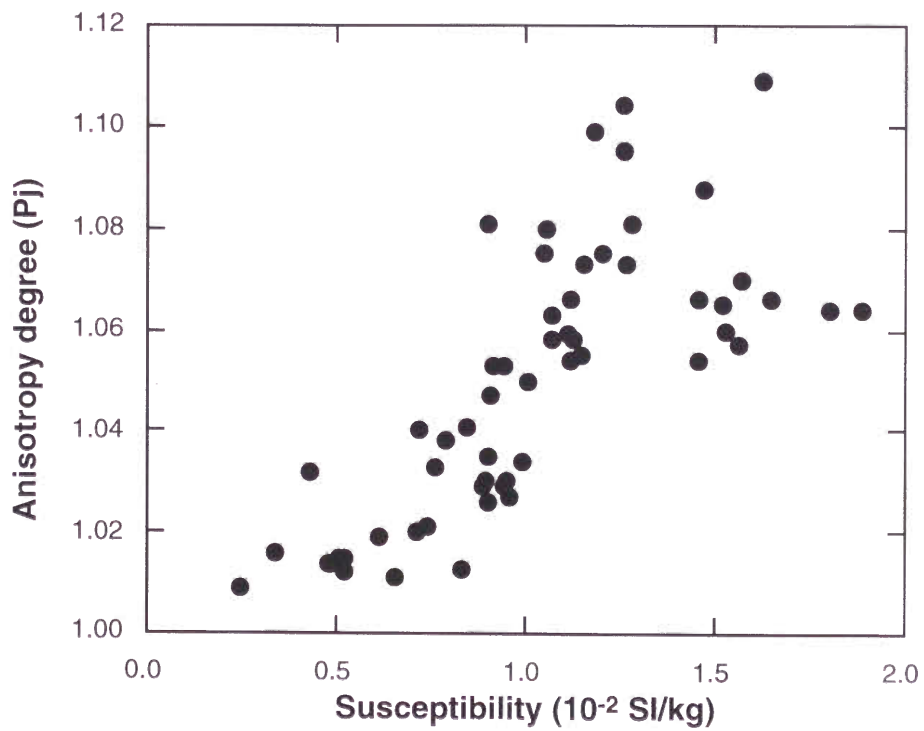

Figure 28. Plot of anisotropy degree of magnetic susceptibility (Pj) to low-field susceptibility. Strong linear correlation are observed.
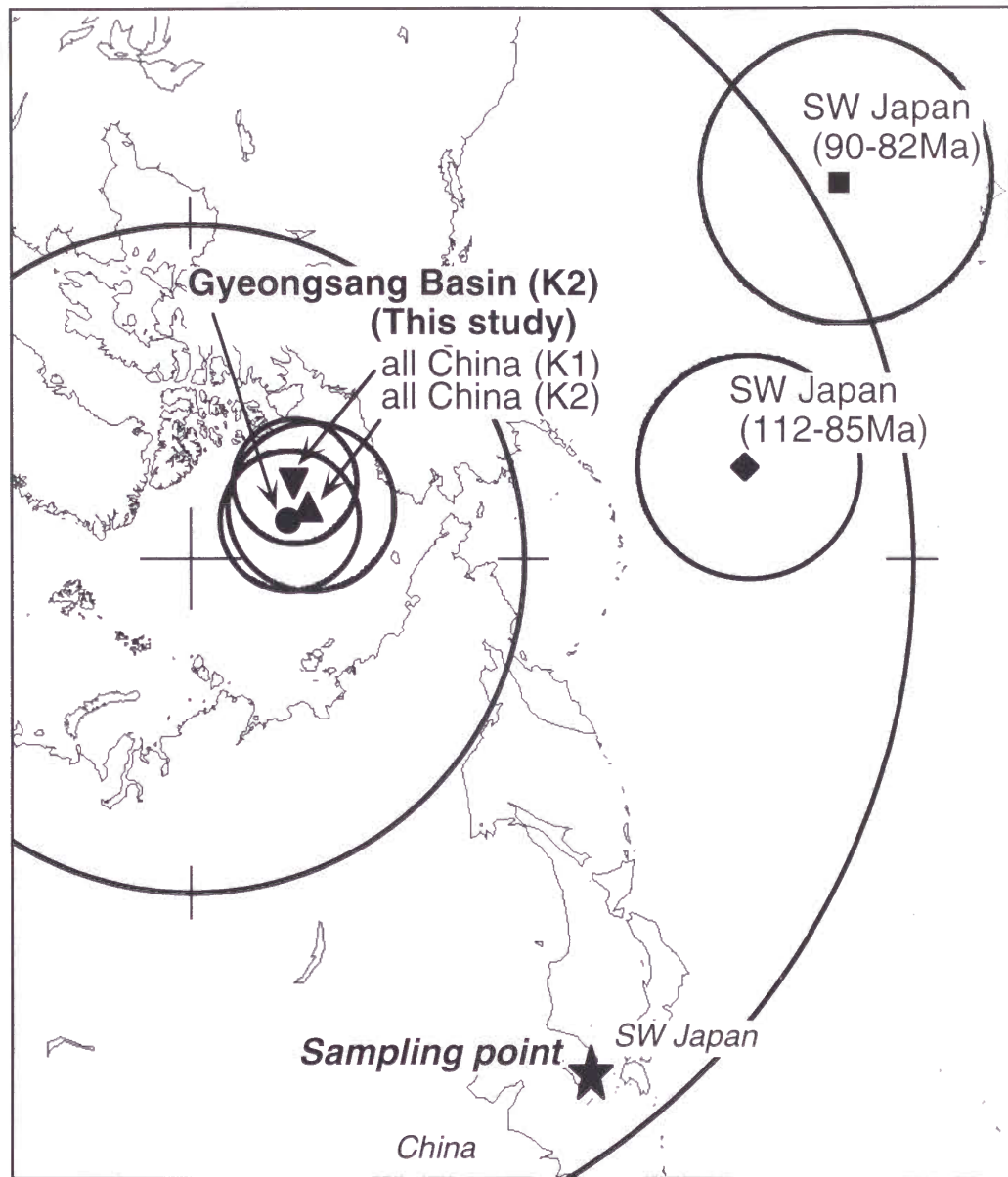
84

Figure 29. Cretaceous paleomagnetic poles with 95% confidence limits from the Gyeongsang Basin and its vicinity, listed in Table 7, on the stereographic projection.